Atmos. Chem. Phys. Discuss., 15, 7585–7643, 2015
www.atmos-chem-phys-discuss.net/15/7585/2015/
doi:10.5194/acpd-15-7585-2015

Atmospheric Chemistry and Physics Discussions

On the radiative impact of aerosols on photolysis rates: comparison of simulations and observations in the Lampedusa island during the ChArMEx/ADRIMED campaign

S. Mailler[1,2], L. Menut[1], A. G. di Sarra[3], S. Becagli[4], T. Di Iorio[3], P. Formenti[5], B. Bessagnet[6], Régis Briant[1], J. Luis Gómez-Amo[3,7], M. Mallet[8], Géraldine Rea[1], G. Siour[5], D. M. Sferlazzo[9], R. Traversi[4], R. Udisti[4], and S. Turquety[1]

[1]Laboratoire de Météorologie Dynamique, IPSL, CNRS, Ecole Polytechnique, École Normale Supérieure, Université Paris 6, UMR8539 91128 Palaiseau CEDEX, France
[2]École Nationale des Ponts et Chaussées – Paristech, Cité Descartes, 6–8 Avenue Blaise Pascal, 77455 Champs-sur-Marne, France
[3]ENEA, Laboratory for Earth Observations and Analyses, Via Anguillarese 301, 00123 Roma, Italy
[4]Department of Chemistry, University of Florence, Sesto Fiorentino, Florence, 50019, Italy

[5]LISA (Laboratoire Inter-Universitaire des Systèmes Atmosphériques), UMR CNRS 7583, Université Paris Est Créteil et Université Paris Diderot, Institut Pierre Simon Laplace, Créteil, France
[6]National Institute for Industrial Environment and Risks (INERIS), Parc Technologique ALATA, 60550 Verneuil-en-Halatte, France
[7]Dpt. Earth Physics and Thermodynamics, University of Valencia. Dr. Moliner, 50, 46100, Burjassot, Valencia, Spain
[8]Laboratoire d'Aérologie, Observatoire Midi-Pyrénées, 14 Avenue Edouard Belin, 31400 Toulouse, France
[9]ENEA, Laboratory for Earth Observations and Analyses, Contrada Grecale, 92010, Lampedusa, Italy

Received: 25 November 2014 – Accepted: 13 February 2015 – Published: 11 March 2015

Correspondence to: S. Mailler (sylvain.mailler@lmd.polytechnique.fr)

Published by Copernicus Publications on behalf of the European Geosciences Union.

ACPD
15, 7585–7643, 2015

Abstract

The Mediterranean basin is characterized by large concentrations of aerosols from both natural and anthropogenic sources. These aerosols change the optical properties of the atmosphere, therefore affecting tropospheric photochemistry through the photolytic rates. Two simulations of the atmospheric composition at basin-scale have been performed with the CHIMERE chemistry-transport model for the period from 1 June to 15 July 2013 covered by the ADRIMED campaign, a campaign of intense measurements in the western Mediterranean basin. One simulation takes into account the radiative effect of the aerosols on photochemistry, the other one does not.

These simulations are compared to satellite and ground-based measurements, with a particular focus on the area of Lampedusa. Values of the Aerosol Optical Depth (AOD) are obtained from the MODIS instrument on the AQUA and TERRA satellites as well as from stations in the AERONET network and from the MFRSR sun photometer deployed at Lampedusa. Additional measurements from instruments deployed at Lampedusa either permanently or exceptionnally are used for other variables: MFRSR sun photometer for AOD, diode array spectrometer for actinic fluxes, LIDAR for the aerosol backscatter, sequential sampler for speciation of aerosol and Brewer spectrophotometer for the total ozone column. It is shown that CHIMERE has a significant ability to reproduce observed peaks in the AOD, which in Lampedusa are mainly due to dust outbreaks during the ADRIMED period, and that taking into account the radiative effect of the aerosols in CHIMERE improves considerably the ability of the model to reproduce the observed day-to-day variations of $J(O^1D)$ and $J(NO_2)$. While in the case of $J(O^1D)$ other variation factors such as the stratospheric ozone column are very important in representing correctly the day-to-day variations, the day-to-day variations of $J(NO_2)$ are captured almost completely by the model when the optical effects of the aerosols are taken into account.

Finally, it is shown that the inclusion of the direct radiative effect of the aerosols in the CHIMERE model leads to reduced $J(O^1D)$ and $J(NO_2)$ values over all the simulation

ACPD
15, 7585–7643, 2015

domain, which ranges from a few percents over continental Europe and the northeast Atlantic Ocean to about 20 % close to and downwind from saharan dust sources. The effect on the modelled ozone concentration is twofold, with the effect of aerosols leading to reduced ozone concentrations over the Mediterranean Sea and continental Europe, close to the sources of NO_x, and on the contrary to increased ozone concentrations over remote areas such the Sahara and the tropical Atlantic Ocean.

1 Introduction

The Mediterranean region is subject to large aerosol concentrations due to both anthropogenic and biogenic emissions. These large aerosol concentrations affect the radiative transfers in the Mediterranean atmosphere through the direct, semi-direct and indirect effect of the aerosols. In Lampedusa, the largest contributors to this effect are the desert dust emissions from the Sahara, the polluted air masses mostly coming from continental Europe, the sea-salt particles emitted either in the Mediterranean Sea itself or advected from the Atlantic, and the particles from biomass burning, when large forest fires occur in southern Europe (Pace et al., 2006). Over the sea surface and in the neighbouring coastal areas, the contribution of sea-spray aerosols is dominant within the boundary layer. Apart from their effect on human health and on the radiative budget of the atmosphere, recent studies (Casasanta et al., 2011; Gerasopoulos et al., 2012) have shown that the radiative effect of the aerosols significantly modulates the photolytic rates in the Mediterranean region. Casasanta et al. (2011) mention a reduction of 62 % in $J(O^1D)$ for a unit Aerosol Optical depth (AOD) at 416 nm when the zenith angle is 60°. The long-term study of Gerasopoulos et al. (2012), with measurements of $J(O^1D)$ and $J(NO_2)$ for a five-year period above the island of Crete showed that, for a constant zenith angle (SZA = 60°), $J(NO_2)$ has an annual cycle that reaches about 15 % of its average value, and that this annual cycle is essentially driven by the seasonal variations in the composition and optical depth of aerosols. At 60° zenith angle, these authors show that a statistically significant correlation exists between the pho-

ACPD
15, 7585–7643, 2015

tolytic rates and the AOD, with a reduction of about 10 % in both $J(NO_2)$ and $J(O^1D)$ for an AOD of 0.3 at a zenith angle of 60°, and about 25 % for an AOD of 0.7. In particular, mineral dust causes significant absorption in the wavelength between 300–400 nm, which are determinant in tropospheric photochemistry (Savoie et al., 2000; Diaz et al., 2001; Kaufman et al., 2001). Even though the aerosols impact the tropospheric photochemistry in several ways, including radiative effects as well as heterogeneous chemistry (Bian et al., 2003), we will focus in this study on the direct radiative impact of aerosols on photolysis rates. It has been shown in the past (Bian et al., 2003) that this effect modifies the global budgets of O_3 and other gases, and that this effect is twofold, leading to reduction of the ozone concentrations in the troposphere in the high-NO_x, ozone producing regions, and increases of ozone concentrations over the low-NO_x regions, particularly over the oceans.

In order to be able to evaluate and take into account the effect of aerosols on photochemistry over the Mediterranean area, a model for radiative transfer and online calculation of photochemical rates, Fast-JX (Wild et al., 2000; Bian et al., 2002), which is already used in various CTMs (Telford et al., 2013; Real and Sartelet, 2011) has been included into the CHIMERE chemistry-transport model (Menut et al., 2013; Mailler et al., 2013). With this new development, the CHIMERE model is able to simulate the radiative impact of aerosols on photochemistry. The Fast-JX module takes into account the values provided in real time by the CTM for all aerosol species as well as for tropospheric ozone up to the top of the CHIMERE domain. The real-time model values of the meteorological variables (temperature, pressure and cloud cover) are also used by the Fast-JX module. Monthly climatological distributions for stratospheric ozone are taken from the McPeters et al. (1997) climatology. As the CHIMERE model takes into account all the major anthropogenic and natural sources of aerosols and trace gases in a realistic way for the Mediterranean basin (Menut et al., 2015), the CHIMERE model including the Fast-JX module, as used in the present study, is an adequate tool to investigate the impact of the aerosols on photochemistry at least for the Mediterranean basin.

ACPD
15, 7585–7643, 2015

In the framework of the ChArMEx (the Chemistry-Aerosol Mediterranean Experiment, http://charmex.lsce.ipsl.fr) campaign, a special operation period, ADRIMED (Aerosol Direct Radiative Impact in the Mediterranean), has been conducted during the summer of 2013. Special Operation Period 1a (SOP1a) lasts from 12 June to 5 July, covering the central part of the simulated period. Various observational data, including photolysis rates $J(O^1D)$ and $J(NO_2)$ at the Lampedusa supersite, are available for this period, during which various episodes of desert-dust intrusions in the free troposphere above Lampedusa have occured. For the 45 days from 1 Juneto 15 July 2013, two simulations have been performed for an area covering the Mediterranean basin, continental Europe and the northern part of Africa. The first simulation (REF) is described and validated in Menut et al. (2015). It includes emissions from mineral dust, biomass burning, anthropogenic and biogenic sources, as well as the radiative effect of aerosols on photochemistry. A second simulation, which we will refer to as NA (no aerosol radiative effect) is performed with exactly the same meteorology, the same emission for aerosols and trace gases, but artificially cancelling the radiative effect of aerosols by setting the real part of their refractive index to 1 and the imaginary part to 0 in the radiative transfer model, making them perfectly transparent at all wavelengths. Therefore, the differences between these two simulations reflect the direct radiative effect of aerosols on photochemistry in the CHIMERE model.

Section 2 exposes the modelling strategy used in both simulations for meteorology, atmospheric chemistry and the radiative transfers, as well as the observational data and techniques. Section 3 presents the validation of the REF simulation by comparison to AOD observations from satellite as well as from ground stations. Descriptions of the vertical structure and speciation of aerosols above Lampedusa as simulated and as observed by the measurement facilities at Lampedusa are also presented. The simulated photolytic rates $J(O^1D)$ and $J(NO_2)$ from both simulations are also compared to the values observed at Lampedusa in order to find whether taking into account the optical effects of aerosols improve the representation of $J(O^1D)$ and $J(NO_2)$ in the CHIMERE model. That section also contains an evaluation of model sensitivity to the

ACPD
15, 7585–7643, 2015

optical depth of aerosols regarding the concentration of ozone over the whole simulation domain. Finally, Sect. 4 sums up and discusses the results obtained in Sect. 3.

2 Data and methods

2.1 Models

2.1.1 Meteorology and atmospheric chemistry

Meteorology has been modelled using the WRF model (Michalakes et al., 2005), version 3.5.1, as described in Menut et al. (2015). The meteorological model is forced by and nudged by the global fields of NCEP/GFS. Meteorological input fields have been produced for the same domain as the CHIMERE simulation domain, which is shown on Fig. 3. The WRF model has been run with 28 vertical levels from the surface to 50 hPa, and a horizontal resolution of 60 km. For the island of Lampedusa, the WRF fields for temperature and wind module are shown here and compared with the field data from the Lampedusa supersite Fig. 1. The modelled temperature has a significant low bias, and lacks a daily cycle compared to the in-situ data, which has pronounced daytime maxima of the temperature. These differences are consistent with the fact that, at the model resolution of 60 km, the island of Lampedusa is not resolved, so that the modelled values reflects open-sea temperature, which is expected to have a much weaker diurnal cycle. Regarding the wind-module, which is a key parameter in modelling sea-salt emissions, Fig. 1b shows that the agreement between model and data for this parameter is quite good, even if for some periods of strong wind, as it is the case from 23 to 27 June for example, the model tends to underestimate the wind module.

The atmospheric chemistry has been modelled with the CHIMERE chemistry transport model (Menut et al., 2013). We used the MELCHIOR-2 chemical mechanism along with the aerosol scheme by Bessagnet et al. (2004). For this study, the emissions are

ACPD
15, 7585–7643, 2015

taken from the HTAP inventory provided by the EDGAR team[1], the boundary conditions for all gaseous and particulate species are taken from LMDZ-INCA climatology (Hauglustaine et al., 2004), except mineral dust which is taken from the GOCART2 climatology (Ginoux et al., 2001), which gives the dust climatology with 7 size bins instead of 3 for LMDZ-INCA. This simulation includes the representation of forest fire emissions, as described in Turquety et al. (2014). Dust emissions have been simulated as explained in Menut et al. (2015), following the Marticorena and Bergametti (1995) scheme for saltation and Alfaro and Gomes (2001) for sandblasting.

Vertical discretization is on 20 levels, with 10 layers below 800 hPa and 10 layers between 800 hPa and the model top, which is placed at 300 hPa. The lowest model layer has 3 hPa thickness, and all the levels between 800 and 300 hPa have equal thickness (60 hPa per layer). This vertical discretization has been chosen to permit a fine representation of both the boundary layer and the free troposphere. The radiative transfers from 300 hPa upward are modelled using climatological ozone concentrations.

The discretization of the particle size distribution of the aerosols is performed over 10 size bins, from 39 nm to 40 µm following a geometric progression with ratio 2, as shown in Table 1.

2.1.2 Actinic fluxes and photolysis rates

The photolysis rates have been calculated using the Fast-JX model, version 7.0b (Wild et al., 2000; Bian et al., 2002). At each time step and in each grid cell, this model resolves the radiative transfers in the model atmospheric column, computing the actinic fluxes at each model level and integrating them over N wavelength bins in order to produce accurate photolysis rates. For our study, N is set to 12, which is the value recommanded by Fast-JX developers for tropospheric studies. These 12 wavelength bins include the 7 standard Fast-J wavelength bins from 291 to 850 nm, as described in Wild et al. (2000). The 7 standard Fast-J wavelength bins are essentially concen-

[1] http://edgar.jrc.ec.europa.eu/htap_v2

ACPD
15, 7585–7643, 2015

trated from 291 to 412.5 nm which is the spectral band relevant for tropospheric photochemistry. Following the recommandations of Fast-JX model developers, 5 additional wavelength bands have been used as well, from 202.5 tp 291 nm, but they are only relevant in the upper tropical troposphere which is not included here since the model top is at 300 hPa. The optical properties of the aerosols are treated at 5 wavelength: 200, 300, 400, 600 and 1000 nm. The optical treatment performed includes absorption by tropospheric and stratospheric ozone, Rayleigh scattering, Mie diffusion by liquid- and ice-water clouds, and absorption and Mie diffusion by aerosols.

The radiative indices for the main aerosol species have been taken as provided on the ADIENT project website[2]. The technical and scientific choices are given in the corresponfing technical report by E. J. Highwood[3]. For mineral dust, they are given in Table 2, and taken from the AERONET values of Kinne et al. (2003). From these values, the extinction cross section per particle, single-scattering albedo and first 7 terms of the Legendre expansion of the scattering phase-function are calculated using Michael Mischenko's code (Mischenko et al., 2002), assuming log-uniform distribution within each diameter bin, and used as input of the Fast-JX radiative code. As in Bian et al. (2003), we chose to neglect the influence of relative humidity on the optical properties of mineral dust and other aerosol species, even though it is well-known that at high relative humidity the influence of water vapor uptake by aerosols might significantly change their optical properties (Flores et al., 2012). Treatment of clouds by Fast-JX is described in, e.g., Wild et al. (2000); Bian et al. (2002). It is worth noting that the simulation period has been largely dominated by conditions with no cloud cover over Lampedusa. However, the spectrometer measurements show that thin clouds occured on 6, 7, 10, 11, 13, 14, 24 June and on 4, 5 July during daytime above Lampedusa.

The photolysis rates in CHIMERE are updated every 5 min by calling the Fast-JX model. The AOD for each model layer is an intermediate result of the Fast-JX model,

[2]http://www.reading.ac.uk/adient/refractiveindices.html

[3]http://www.reading.ac.uk/adient/REFINDS/Techreportjul09.doc

ACPD
15, 7585–7643, 2015

which we sum over the model layers and export for the 5 wavelengths used by Fast-JX in order to compare it to available observations.

One key parameter in simulating $J(O^1D)$ is the total atmospheric ozone column. Within the simulation domain (from the surface to 300 hPa), Fast-JX uses the online ozone concentrations calculated within CHIMERE. Above this level, that is, for upper tropospheric and stratospheric ozone, Fast-JX uses tabulated climatological ozone concentrations. These climatological concentrations from McPeters et al. (1997), included within the Fast-JX module in its standard configuration, are given with a vertical resolution of about 2 km up to an altitude of about 60 km, with monthly values for every 10° latitude band. For the latitude band corresponding to Lampedusa (30–40° N), the stratospheric ozone column obtained by vertically summing these climatological concentrations amounts to 248.6 DU for the month of June, and 236.4 DU for the month of July. The contribution of tropospheric ozone from the CHIMERE model is of about 30 DU for all the simulation periods. Therefore, the total ozone column taken into account by the radiative transfer model oscillates around 280 DU for the month of June, and 265 DU for the month of July, a value which is far below the measured value above Lampedusa, which evolves within the 300–360 DU range for all the simulation period (Fig. 2). Total ozone is routinely measured at Lampedusa by means of a MKIII Brewer spectrophotometer, as described in Meloni et al. (2005). Figure 2 also shows that the variability of the total ozone column is much smaller in the model than in the observed values, due to the use of a climatological value for the stratospheric ozone column instead of time-varying values. This insufficient stratospheric ozone column is expected to have a significant impact on the modelled $J(O^1D)$ photolytic rates.

2.2 The backplume calculation methodology

In order to understand the origin of several air masses, a simplified backplumes model was developed and used in this study. The main principle is to use the WRF simulation results and to advect back in time numerous passive tracers. For each backplume, a location, a time and an altitude is chosen. The meteorological parameters used are:

ACPD
15, 7585–7643, 2015

– The three-dimensional wind components: u the zonal wind (m s^{-1}), v the meridian wind (m s^{-1}) and w the vertical wind (m s^{-1}).

– The boundary layer height $\overline{h}$ and the surface sensible heat flux Q_0.

For each starting point, one hundred passive tracers are launched. For each one, its back-trajectories are estimated during the previous 120 h, back in time. Three cases are considered for each time and each location:

– In the boundary layer and during a convective period ($Q_0 > 0$): we consider that the particle is in the convective boundary layer. The meteorological fields being available at an hourly time-step, we consider the particle may have been at any level inside the boundary layer the hour before. We thus apply a random function to reproduce vertical mixing within the boundary layer.

– In the boundary layer and during a stable period ($Q_0 < 0$): the particle stays in the boundary layer at the same altitude.

– In the free troposphere: we consider that the particle vertical evolution may be influenced by the vertical wind component. We thus apply a random function to estimate its possible vertical motion with values between $w/2$ and $3w/2$.

2.3 Observational data and techniques

The Lampedusa station is located on the Lampedusa island. Lampedusa is a small island located some 140 km East of the Tunisian coast and about 210 km South-West of the Sicilian coast, so that the aerosol properties at and above Lampedusa can be considered as mainly representative of long-range transport and of marine aerosol (Pace et al., 2006). The measurements available at Lampedusa during the simulated period or at least during part of it include measurements by the MFRSR instrument (Multi Filter Rotating Shadowband Radiometer) for the Aerosol optical depth, a Metcon diode array

ACPD
15, 7585–7643, 2015

spectrometer for actinic flux and photolytic rates, a Brewer spectroradiometer for total ozone column, an aerosol LIDAR, and a low-volume dual-channel sequential sampler.

2.3.1 Remote sensing and radiative measurements

The AERONET (Aerosol Robotic Network, http://aeronet.gsfc.nasa.gov) and MFRSR data was used for the AOD, MFRSR data was also used for calculating $J(NO_2)$ and $J(O^1D)$ at the Lampedusa supersite. The AERONET data was used for three stations: Lampedusa (35.51° N; 12.63° E), Oujda (34.65° N; 1.90° E) and Palma de Mallorca (39.55° N; 2.63° E). Level 2.0 data was used for Oujda and Palma de Mallorca, while only Level 1.5 data was available for Lampedusa. The AOD time series for Lampedusa was completed by MFRSR measurements carried out at the Lampedusa station (Pace et al., 2006; di Sarra et al., 2015) for the periods when the AERONET data were not available, namely 2 to 16 June, and 27 June. The AERONET AOD as well as MFRSR AOD has been linearly interpolated at the wavelength of 400 nm, which is one of the five wavelengths for which Fast-JX computes the AOD. The interpolation was performed linearly, based on the nearest available wavelengths in the measured data, 380 and 440 nm for the AERONET data, 416 and 440.6 nm for the MFRSR data.

Actinic flux spectra were measured using a Metcon diode array spectrometer (Casasanta et al., 2011). The actinic flux measurements were calibrated at the beginning of SOP1a by using NIST traceable 1000 Watt lamps. The value of $J(O^1D)$ was derived from the actinic flux measurements as described by Casasanta et al. (2011). $J(NO_2)$ was calculated from the measured actinc flux spectra by using the temperature dependent NO_2 absorption cross sections by Davidson et al. (1988) and the NO_2 quantum yield from Gardner et al. (1987). It is worth noting that the measured actinic flux, and therefore the photolysis rates, take into account only the downward actinic flux.

The estimated accuracy is about 0.01 for the AERONET AOD, about 0.02 for the MFRSR AOD (Pace et al., 2006), and about 1 % on the total ozone measurements by the Brewer spectroradiometer, which are done routinely at Lampedusa. The estimated

ACPD
15, 7585–7643, 2015

uncertainty is between 5 and 8 % for $J(O^1D)$, depending on the solar zenith angle and occurring conditions, and about 3–4 % for $J(NO_2)$.

An aerosol lidar is operational at Lampedusa, and provides measurements of vertical profiles of the aerosol backscattering at 532 nm. Details on the instrumental setup and on the retrieval method are given by Di Iorio et al. (2009). For this study, one or two daily backscattering profiles, obtained by averaging lidar signal over 5–30 min intervals, are chosen as representative for the occurring conditions on the corresponding day. The vertical resolution of the measurements is 7.5 m.

The AOD from MODIS Aqua and Terra v. 5.1 at 550 nm has been retrieved using the NASA LADS website[4]. Only quality-assured, cloud-screened level 2 data has been used for this study. The expected error envelope for these values are of $\pm 0.05 + 0.15$AOD over land, and $\pm 0.03 + 0.05$AOD over ocean. About 60 % of values (above ocean) and 72 % (over land) fall within this expected error margin (Remer et al., 2008). When available, we use in priority the AOD from the deep-blue algorithm, which permits to have satellite-retrieved values for the AOD even over bright surfaces such as desertic areas. This product has an expected error envelope of $\pm 0.03 + 0.20$AOD (Sayer et al., 2013).

2.3.2 Aerosol concentration and speciation

PM_{10} samples were collected at Lampedusa Island at 12 h resolution by using a low volume dual channel sequential sampler (HYDRA FAI Instruments) equipped with sampling heads operating in accord with the European Norm EN12341 (following Directive 2008/50/EC on ambient air quality and cleaner air for Europe). The mass of PM_{10} was determined by weighting the filters before and after the sampling with an analytical balance in controlled conditions of temperature ($20 \pm 1\,^{\circ}C$) and relative humidity (50 ± 5 %). The estimated error on the basis of balance tolerance for the PM_{10} mass is around 1 % at 30 $\mu g\,m^{-3}$ of PM_{10} in the applied sampling conditions. A quarter of each filter is anal-

[4] ftp://ladsweb.nascom.nasa.gov/allData/51/

ACPD
15, 7585–7643, 2015

ysed for soluble ions content by Ion Chromatography as described in Marconi et al. (2014). The error margin for Ion Chromatographic measurements is of 5 % for all the considered ions.

Na, Cl, Mg, Ca, K and sulphate are the main components of sea-salt aerosol (SSA). As these ions (excluding Cl) have other sources than sea-spray, the sea-salt (ss) fraction of each ions was used to SSA calculation. details on the calculation of sea-salt and non-sea-salt (nss) fraction for Na and Ca by using the ratio Ca/Na in sea water ($(Ca/Na)_{sw}$ = 0.038; Bowen, 1979) and Na/Ca average in the upper continental crust ($(Ca/Na)_{ucc}$ = 0.56; Bowen, 1979) are reported in Marconi et al. (2014). The sea-salt fractions for Mg, Ca, K and sulphate are calculated by multiplying the ssNa by the ratio of each component in bulk sea water: $(Mg/Na)_{sw}$ = 0.129, $(Ca/Na)_{sw}$ = 0.038, $(K/Na)_{sw}$ = 0.036, $(SO_4^{2-}/Na)_{sw}$ = 0.253. For chloride we used the measured concentration instead of the calculation from ssNa, because during the aging of sea spray chloride undergoes a depletion process (Keene et al., 1998), mainly due to reactions with anthropic H_2SO_4 and HNO_3, leading to re-emission of HCl in the atmosphere. Previous work by Kishcha et al. (2011) shows a very good agreement between SSA obtained by DREAM-Salt model and the calculated SSA from chemical composition at Lampedusa.

Dust aerosol is calculated from nssCa as this marker is one of the most reliable of crustal material Putaud et al. (2004); Sciare et al. (2005); Guinot et al. (2007); Favez et al. (2008). Besides, Ca is largely used because it allows the identification and quantification of Saharn dust on the basis of only ion chromatographic measurements. On the other hand, upper continental crust presents a large variability in Ca content. In particular, some areas of the Sahara are enriched in Ca minerals (Scheuvens et al., 2013), leading to an overestimation of crustal material in the aerosol by using only the Ca (or nssCa) in the calculation. In the Mediterranean region, several studies have evaluated and used calcium-to-dust conversion factors to estimate the crustal content (Sciare et al., 2005; Favez et al., 2008). In Lampedusa, over an extensive dataset, (Marconi et al., 2014) found a significant correlation between nssCa and crustal con-

ACPD
15, 7585–7643, 2015

tent computed by the more reliable method of the main crustal element oxides formula. The slope of the regression line (10.0 ± 2 %), which is in the range of previous studies in the Mediterranean region (Sciare et al., 2005; Favez et al., 2008) is used as calcium-to-dust conversion factor in the present study. Finally, non-dust PM_{10} is obtained by subtraction of dust content from PM_{10} total mass.

3 Results

3.1 Comparison of model outputs with observational data

3.1.1 Aerosol optical depth

Figure 3 compares the AOD simulated by CHIMERE at 600 nm to that measured by MODIS at 550 nm, averaged from 1 June to 15 July. It shows that, on average for all the considered period, CHIMERE reproduces realistically the main features of the AOD over the considered region, with average values above unity for the Sahelian band and the Arabian peninsula. However, CHIMERE misses high AOD values on the eastern side of the Caspian Sea as well as over the northern part of the Atlantic, and also underestimates the AOD in eastern Sahara. For the first area, the underestimation of the AOD by CHIMERE may be related to missing dust emissions, while for the northern Atlantic the high AOD values in MODIS are related to an average computed from very few data points, possibly during an event of transport of an aerosol plume (e.g. biomass burning or mineral dust) from outside the simulation domain, or contaminated by the presence of thin clouds in that area.

For the most important part of our domain, including continental Africa, the comparison of the average AOD between CHIMERE and MODIS is rather satisfactory: maxima due to local dust emissions are observed in the Sahara and Sahel, and the climatological dust plume off the coast of West-Africa and above the Cabo-Verde islands is well

ACPD
15, 7585–7643, 2015

captured by the model, even though some underestimation in the model can be seen in this plume.

Over the Mediterranean Sea, average values around 0.2 are modelled by CHIMERE and observed by MODIS, with larger values just off the coasts of North-Africa and a south-north gradient, with smaller AOD values in the northern part of the Mediterranean Sea.

Regarding the time evolution of the AOD, we selected three particular days in June, 17 June, 19 and 21, sampling the dust outbreak that occured between 13 and 25 June over the Western Mediterranean basin, during ADRIMED SOP1a. Figure 4 shows the AOD at 400 nm and at 12 GMT simulated by CHIMERE for these three days, and measured by MODIS for the same dates (MODIS overpass was between 10 GMT and 14GMT over the considered zones for these days).

For 17 June (Fig. 4a and b), the dust plume is visible both in the model and in observations, with maximal AOD values around 0.6 in both cases, even though the plume seems slightly more extended and optically thicker in the model than in the observations. In both model and observations, the maximal AOD for this plume is located over the sea, southwest of the Balearic islands. For 19 June (Fig. 4c and d), the dust plume has moved to the east, just west of Corsica and Sardinia. It extends further to the south in the model than in observations. Finally, on 21 June (Fig. 4e and f), the dust plume is over the Tyrrhenian Sea, also reaching Lampedusa, and has become significantly more intense in the model than in observations.

During the same time period, a zone of strong AOD is present in CHIMERE off the coasts of France, Britain and Ireland (Fig. 4a), then over the Gulf of Gascony (Fig. 4c) and finally on 21 June, a zone of very strong AOD over the North Sea. No MODIS measurements are present at the same time to evaluate this zone of thick aerosols, even though Fig. 4d indicates a zone of strong AOD over the North Sea at that time, consistant with CHIMERE simulation. At that time, it is worth going back to Fig. 3 which shows that, for the time and place where MODIS measurements are available for these marine areas, no overestimation of the AOD by CHIMERE can be seen on average.

ACPD
15, 7585–7643, 2015

A detailed comparison of the AOD with AERONET stations for all the ADRIMED period is presented in Menut et al. (2015). Here, we selected three AERONET stations that have sampled the dust plume we discussed before in order to evaluate the modelled AOD for the considered period.

These three AERONET stations have been selected in the Western Mediterranean according to the data availability for June 2013 and their position on the trajectory of the dust plume of 13–25 June as seen by MODIS. As discussed in Sect. 2, the three selected stations are Lampedusa (Italy), Oujda (Marocco) and Palma de Mallorca (Spain). The AERONET data for Lampedusa was not available for 1 to 16 June, so that the time series have been completed using the MFRSR data at Lampedusa station for those 16 days as well as for 27 June. The comparison of the AOD measured in these three AERONET stations to the AOD of CHIMERE is shown on Fig. 5 at 400 nm.

The dust peak observed from 21 to 24 June in Lampedusa is simulated realistically by CHIMERE (Fig. 5a). The peak value of the AOD is about 0.5 in the model and 0.35 in the observations. Three other sharp peaks in AOD are represented in CHIMERE for 6 June, 9–10 June and 2–4 July. The peak of 6 June is the most intense in the simulation period, and has a rather short duration (about 24 h). The maximal value of the AOD during this peak is between 0.8 and 0.9 in both the MFRSR data and the model in the afternoon of 6 June. The AOD value then decreases steadily on 7 June, ranging between 0.5 and 0.3 in both modelled and measured values for that day. The peak in the afternoon of 9 June, the second most intense in the whole data series (AOD = 0.6) has been sampled by MFRSR, and is present as well in CHIMERE, with a very comparable peak value, reached in the afternoon of 9 June and the following night. The decrease of the AOD values occurs on 10 June, when AOD returns to a value of about 0.2. A last peak in AOD is present in both model and observations from 2 July to 4 July, followed by moderate AOD values, around 0.2, throughout the rest of the simulation period.

For the Oujda station (Fig. 5b), a peak in AOD is represented in both the model and observations from 12 to 17 June, with a similar timing and duration between the

ACPD
15, 7585–7643, 2015

model and the observations and a stronger value for the maximal AOD in the model than in observations (0.6 vs 0.4). Another strong AOD peak is simulated by CHIMERE from 28 June to 2 July, but with no available data at the time, and a last AOD peak is modelled and observed on 11–12 July. The background value of the AOD (about 0.05–0.1) for this location is represented realistically by CHIMERE. Finally, for the Palma de Mallorca station (Fig. 5c), a very brief peak in AOD is simulated in CHIMERE for 7 June, but not seen in the AERONET time series because it occurs in nighttime. Thereafter, a peak from 16 to 18 June with AOD reaching 0.5 in CHIMERE and 0.3 AERONET is simulated and observed. A significant AOD peak from 25–30 June is observed but missed by the model. A last AOD peak is simulated and observed on 2–3 July, and a trend towards higher AOD values can be seen in both the model and observations towards the end of the period.

All in all, it can be seen that the AOD values simulated by CHIMERE over the western Mediterranean compare well to observations from MODIS, AERONET and MFRSR, and that the peaks simulated by CHIMERE during that period are generally observed except when they occur during nighttime, as it is the case for the night of 7–8 June at Palma de Mallorca. Only one significant AOD peak is observed but missed by the model, from 25–30 June at Palma de Mallorca, while the model catches all the AOD peaks that occur at Lampedusa and Oujda during the simulation period. The longest dust transport event of this period (12–24 June) is represented realistically for all three locations, first in Oujda, therafter in Palma de Mallorca, and finally at Lampedusa, even though for these three locations the peak value of the AOD is stronger in CHIMERE than in the observations. Therefore, the period of time from 1 to 15 June 2013 is suitable to examine the impact of aerosol loads on photochemistry in CHIMERE, taking advantage of the availability of measurements from the ADRIMED SOP1a period.

3.1.2 Vertical structure

The episodes of dust incursion visible on the simulated AOD time series (Fig. 5a) can also be seen in the time-altitude simulated particles concentrations, see Fig. 6a for

ACPD
15, 7585–7643, 2015

coarse particles (PM_{10}–$PM_{2.5}$) and Fig. 6b for fine particles ($PM_{2.5}$). Dust is present above Lampedusa in the simulation outputs from 4 to 10 June, from 19 to 28 June, from 1 July to 4 July, and from 11 July to 15 July (Fig. 6a). A significant amount of finer particles is also present in the boundary layer during most of the simulation period, particularly from 11 to 20 June, while maxima of $PM_{2.5}$ concentration occur in the free troposphere as well during the dust outbreaks. Lidar profiles have been selected once or twice a day for comparison to the model (Fig. 6c). In these LIDAR measurements of backscatter coefficient, aerosol plumes in the free troposphere are clearly visible from 8 to 10 June, from 19 to 28 June, and from 2 July to 4 July. These aerosol plumes in the troposphere are seen between 2000 and 6000 m altitude, consistent with the altitudes of the PM_{10} maxima simulated in CHIMERE. The first event sampled in the LIDAR data, between 8 and 10 June, occurs at a low altitude, with a concentration maximum between 1000 and 2000 m a.g.l. in both measurements and simulation. During the same period, a strong backscatter signal is also observed in the boundary-layer, corresponding to the maxima of fine particle concentrations in the boundary-layer, this boundary-layer contribution being dominant when there is no significant contribution from dust in the free troposphere, which is the case from 11 to 19 June (Fig. 6b). Modeled profiles display a structure very similar to observations. However, it must be pointed out that the modeled dust plume reaches generally higher altitudes, up to about 8 km, than observations.

3.1.3 Speciation

For the simulation period, the speciation of the particulate matter in the first model layer (Fig. 7) is shown. For the first model layer, a comparison of PM_{10} speciation has been performed between the model and the measurements, for three categories of aerosols: total PM_{10}, non-dust PM_{10}, and SSA PM_{10}. It is worth noting at that point that, even though the Lampedusa station is located at an altitude of 45 m.a.s.l., we compared the measured concentrations to the concentrations modelled for the first modelled level (0–30 m) rather than the second model level (30–70 m). We lack small-

ACPD
15, 7585–7643, 2015

scale meteorological information to know whether the air masses that arrive at the measurement station come from the first 30 m above the sea, or from air particles that were already at about the altitude of 45 m during their travel above open sea. However, we checked that the modelled concentrations of the various aerosol species above Lampedusa do not change measurably between the first and the second model layer (not shown), so that the results discussed here are not sensitive to that choice.

For total PM_{10} (black lines), the agreement between modelled and measured value is not good, with a large overestimation of aerosol concentration by CHIMERE (the average value for all the times where measured values are available is 41.9 $\mu g\,m^{-3}$ in CHIMERE against 18.8 $\mu g\,m^{-3}$ in the measurements), with a significant but moderate temporal correlation (correlation coefficient of 0.40). Results for non-dust PM_{10} (blue lines) are much better. Even though the bias in CHIMERE is still strong (31.7 $\mu g\,m^{-3}$ in CHIMERE against 17.6 $\mu g\,m^{-3}$ in the measurements), the temporal correlation ($R = 0.72$). The better agreement in non-dust PM_{10} between the model and the measurements permits to conclude that the poor agreement between model and observations for total PM_{10} is in part due to an overestimation of dust concentrations in the first model layer by CHIMERE. Given the vertical structure of the dust layers, that are essentially located in the free troposphere (Fig. 6), this large overstimation of dust concentrations at ground level in Lampedusa may be an indicator of excessive deposition and/or numerical diffusion in the model compared to reality.

If we now examine the time-series for sea-salt aerosols (Fig. 7, green lines), there is a very good temporal correlation between CHIMERE and the measured values ($R = 0.90$), showing that the evolution of the sea-salt concentration is very well captured by the model. However, a significant bias in modelled values relative to the observations can be observed, due to the presence in the model of a significant background concentration of sea-salt: while the modelled sea-salt concentrations almost always exceed 5 $\mu g\,m^{-3}$, the measured values get very close to 0 in some periods, for example between 15 and 20 June, a period of very weak wind (Fig. 1b) during which the model tends to overestimate the wind. This overestimation of the wind during periods

ACPD
15, 7585–7643, 2015

of weak winds can be a factor explaining the excessive backgroung sea-salt concentration. As a summary, simulated PM_{10} in the boundary layer are overestimated by $5\,\mu g\,m^{-3}$ in average in the bounadry layer at Lampedusa. This overestimation comes from the mineral dust ($8\,\mu g\,m^{-3}$), the sea-spray aerosols ($5\,\mu g\,m^{-3}$) and other aerosols ($9.5\,\mu g\,m^{-3}$).

Regarding the total aerosol column (Fig. 8), it is generally largely dominated by dust, with dust loads reaching 1–2 $g\,m^{-2}$ during a sharp peak, and a background level around or below $0.1\,g\,m^{-2}$. Therefore, mineral dust is the dominant contributor to the AOD for Lampedusa at least during AOD peaks. At Lampedusa, the other aerosol species contribute to the tatal aerosol load by at least one order of magnitude less than mineral dust. this is the case of ammonium, sulphates sea-salts and Primary anthropogenis particulate matter ($\simeq 0.01$–$0.1\,g\,m^{-2}$), while all the other species contribute again one order of magnitude less.

The fact that the AOD in Lampedusa as well as other stations is represented in a realistic way by the model (Fig. 5a) is an indication that the total aerosol loads represented by CHIMERE are realistic. The LIDAR measurements in Fig. 6b and c also confirm that the aerosols in the free troposphere, where dust is dominant (Fig. 8), seem to have a stronger contribution to the total backscatter than aerosols located in the boundary layer, where non-dust aerosols generally dominate (Fig. 7). In that sense, both model and measurements seem to indicate that the dominant contribution to the AOD during the considered period can be attributed to the presence of dust in the free troposphere, at least during periods of AOD peaks. The boundary-layer aerosols such as sea-salt and other species might have a significant contribution to the background AOD values in periods when dust is almost absent from the troposphere above Lampedusa, as it is the case between 12 and 18 June for example.

Finally, in order to understand the source regions of the aerosols modelled and observed above Lampedusa, we performed a backtrajectory study for two particular times and altitudes (Fig. 9). 23 June, 12:00 UTC at 4500 m altitude, is a point selected inside a free tropospheric dust layer (Fig. 6), and 24 June, 12:00 UTC at 10 m.a.g.l., corre-

ACPD
15, 7585–7643, 2015

sponds to a zone of strong sea-salt concentration in the marine boundary layer (Fig. 7). Figure 9a shows that the air masses arriving at 4500 m above Lampedusa on 23 June at 12:00 UTC were all located above north-Africa from 72 to 24 h before their arrival. Over these arid areas where they stayed for several days being caught in the boundary layer every day and detrained every night (Fig. 9c), they gained a significant content in mineral dust particles likely due to local emissions. These dust particules are then advected to the vertical of Lampedusa, being in the free troposphere during the last 72 h of their travel. If we now look at the backtrajectories of the air masses contributing to the strong sea-salt content on 23 June at 12:00 UTC in the lowest layers (Fig. 7), the backtrajectories (Fig. 9b) show that these particles come from the northwest and have travelled 24 h or more above the western Mediterranean, smost of them staying inside the marine boundary layer all along their trajectory (Fig. 9d). These trajectories are consistent with the backtrajectories given by Pace et al. (2006) for days with a strong sea-salt content at Lampedusa, and provide a particularly long trajectory of this air mass above water, which favours sea-salt emissions (Granier et al., 2004).

As a balance of this section, it can be said that:

- The average AOD over the whole simulation domain is simulated correctly by CHIMERE for the considered time period (1 June to 15 July), and compares favorably to MODIS AOD.
- The dust plume simulated by CHIMERE over the western Mediterranean from 13 to 25 June is also captured by MODIS, as well as by the relevant AERONET stations. It has been observed by the LIDAR in Lampedusa at about the same time and altitude as modelled in CHIMERE. The AOD values simulated are realistic, as well as the eastward movement of the plume and its timing at each of the measurement stations.
- At Lampedusa, measurements of the chemical composition of aerosols show that the dust plume has not reached the ground level during the simulation period, which is contrary to the simulation outputs. This overestimation of dust concen-

ACPD
15, 7585–7643, 2015

tration in the boundary layer might be a consequence of excessive numerical diffusion in the model, as discussed in Vuolo et al. (2009).

3.2 Impact of aerosols on photolysis rates at Lampedusa

3.2.1 Comparison of modelled $J(NO_2)$ to observations

Figure 10a shows the time series of the daily maxima of $J(NO_2)$ in both simulations as well as the $J(NO_2)$ value derived from the Metcon spectrometer measurements at Lampedusa. The measurements take into account only the downward contribution to the actinic flux, while the modelled value also includes the upward flux due to the non-zero albedo of the surface. Since the albedo of the surface in the model has been set to a fixed value of $A = 0.1$ for this simulation, we multiplied the modelled value for $J(NO_2)$ by a correction factor of $1/(1 + A)$ in order to obtain a modelled $J(NO_2)$ value plotted in Fig. 10a, which is representative of the downward component of the actinic flux only and can therefore be compared directly to the measured values. It is worth noting that the simulation period is centered on the summer solstice, so that the Solar zenith angle at local solar noon only varies from 12.94° on 6 June to 12.07° on 21 June. The cosine of that angle (which determines the optical path of incoming solar rays inside the atmosphere) only varies by about 0.3 % during the measurement period. This explains the fact that no seasonal trend is visible either in the model or in the measurements, and needs not be taken into account for our study. Similarly, changes in the Sun–Earth distance are very small, and produce a negligible effect on the day-to-day variations in the selected period. Thin clouds were present above the station on 6, 7, 8, 10, 11, 13, 14, 24 June and on 4 and 5 July. These days are signalled on Fig. 10a by empty diamonds, while days when no cloud influence exists in the measurements are represented by full diamonds. In the model, cloud cover was present over Lampedusa in daytime only on 5, 27 and 30 June and 5 July. However, it is visible on Fig. 10a and b that these clouds were not thick enough to influence the photolytic rates above Lampedusa.

ACPD
15, 7585–7643, 2015

Two observations can be made from Fig. 10a. First, that the values of diurnal maxima of $J(NO_2)$ in both simulations are positively biased. This bias is of 12.3 % for the simulation without aerosols (NA), and 8.2 % in the reference simulation. The second observation is that the variations of the daily maxima of $J(NO_2)$ in the REF simulation correspond almost exactly to these of the measured data: calculating the linear correlation between these two time series yields a correlation coefficient of 0.92 and a slope of 1.13 (Table 3), both representing an excellent correlation between the simulated and measured daily maxima of $J(NO_2)$. This excellent correlation indicates that the variations of $J(NO_2)$ due to the optical effect of aerosols are very well represented in this simulation. This result clearly shows that taking into account the optical effect of aerosols gives a strong added value in the capacity of a model to reproduce day-to-day variations in the photolytic rates.

It is also interesting to examine the representation of the diurnal cycles of $J(O^1D)$ and $J(NO_2)$ in CHIMERE for both clear days and days with a moderate AOD. For that purpose, based on AOD value and data availability, we selected 18 June as a representative clear-sky day, and 23 June as a day representative of a moderate dust outbreak. Measured AOD value is about 0.1 for 18 June, and modelled AOD about 0.12 for the same day, while for 23 June, measured AOD is about 0.35 and modelled AOD is about 0.45 in average. Figure 11a shows the simulated and observed diurnal cycle of $J(NO_2)$ for these two days. For 18 June (Fig. 11a), it can be seen that the values in the morning and the evening are simulated very realistically by both simulations, while both simulations overestimate $J(NO_2)$ around local noon. For 23 June, the time evolutions of measured $J(NO_2)$ have variations from an hour to another. The modelled $J(NO_2)$ values in the REF simulations does not have such variations, suggesting that the spatial resolution of the CHIMERE model and the smoothing of dust plumes by numerical diffusion lead CHIMERE to miss some fine-scale spatial structures of the plume. Despite this lack of rapid variations, the REF simulation does much better than the NA simulation in representing $J(NO_2)$ for that day. The simulated values for the REF simulations are either stronger or weaker than the measured values, depending

ACPD
15, 7585–7643, 2015

on the hour. The systematic overestimation of $J(NO_2)$ by the model around local noon is still present for that day, but the model bias is much weaker in the REF simulation than in the NA simulation.

A scatter plot of modelled vs. observed $J(NO_2)$ values (12a) confirms that the relationship between observed and modelled $J(NO_2)$ values is excellent for both simulations, even though discrepancies between observed and simulated values are stronger in the NA simulation than in the REF simulation. The correlation coefficient (Table 3) is higher in the REF simulation (0.993) than in the NA simulation (0.987), being excellent in both cases. Since $J(NO_2)$ is essentially a function of the solar zenith angle, these very high correlation coefficients primarily show that the dependence of $J(NO_2)$ on the solar zenith angle is represented very well by the CHIMERE model.

3.2.2 Comparison of modelled $J(O^1D)$ to observations

Figure 10b shows the time series of the daily maxima of $J(O^1D)$ for both the REF and the NA simulation as well as in the measurements when available.

Comparison of the daily maxima between the REF and the NA simulation shows that the effect of the aerosols above Lampedusa on the $J(O^1D)$ for that period reduces the daily maximum of $J(O^1D)$ by 3 to 20 %, depending on the AOD. The minimal value of the daily maximum $J(O^1D)$ is reached on 6 June, both in the REF simulation and in the observations, possibly due to a sharp peak in AOD for that day (Fig. 5a). The peak in modelled dust load and in simulated and observed AOD between 20 and 25 June (Fig. 5a) generates another period of strong impact of aerosols on $J(O^1D)$, both in the model and in the observations.

From a statistical point of view (Table 3), the NA simulation, without the direct effect of the aerosols, has no ability to reproduce the day-to-day variations of $J(O^1D)$ ($R = 0.09$, p value = 0.65). On the contrary, the REF simulation, including the aerosol direct effect, has a correlation coefficient of 0.46 to the observations, and a p value of 0.02 that gives good confidence in this result despite the reduced size of the sample (26 points).

ACPD
15, 7585–7643, 2015

This shows that taking into account the direct optical effect of the aerosols permits to CHIMERE to better represent the measured day-to-day variations of $J(O^1D)$.

The correlation coefficient of daily maxima in $J(O^1D)$ between the REF simulation and the observed values is only 0.46, much lower than the value of 0.92 obtained for $J(NO_2)$ correlation. This lower value can be explained by the fact that, even when clouds are not present, $J(O^1D)$ is influenced by other factors than the AOD, and first of all by the total ozone column. From that point of view, the period for which measurements of $J(O^1D)$ are available, from 5 June to 5 July, can be separated into two periods according to the total ozone column (Fig. 2). In the first half of June, until 13 June, the values of ozone column oscillate around 340 DU, in the second half of June and the beginning of July, it oscillates around 310 DU. This transition is reflected on Fig. 10b by stronger $J(O^1D)$ value after 14 June than before 13 June, corresponding to a thinner ozone column. This large variation of the measured $J(O^1D)$ values is not captured by the model, which uses prescribed values for stratospheric ozone. The dependence on temperature is also a possible explanation of the disfferent variations between the observed and modelled $J(O^1D)$ values, since the modelled temperature values in the boundary layer are not representative of the local temperature at Lampedusa (Fig. 1). On the contrary, $J(NO_2)$ has only a marginal dependence on the total ozone column, which explains the very high correlation coefficient obtained between the observed and modelled values (0.92). Therefore, the moderate correlation of daily maxima of $J(O^1D)$ (0.46) between modelled and observed values must not be blamed on a bad representation of aerosols in the model, but rather on the absence of variations of the stratospheric ozone column in the model.

As for $J(NO_2)$, we will examine the diurnal cycles for 18 and 23 June, considered as representative of clear days and days with a strong AOD, respectively. If we first look at the clear-sky measured and modelled diurnal cycles, (Figs. 11c), as could be expected, we see that the simulated $J(O^1D)$ values in the NA simulation are barely different from those in the REF simulation, revealing a very small impact of the AOD on photolytic rates for that day. Comparison of simulated $J(O^1D)$ to the observed values (Fig. 11c)

ACPD
15, 7585–7643, 2015

shows that both simulation simulate quite realistically the observed $J(O^1D)$ for that day, with a slight underestimation of $J(O^1D)$ by the model, particularly around local noon. The general shape of the diurnal cycle of $J(O^1D)$ is captured very well by the model. For 23 June, on the contrary, the REF and the NA simulations are very different due to the strong dust column. Compared to 6 June, the reduction in $J(O^1D)$ is strong for both the REF simulation (11 % at local noon noon) and the measured values (7 %). It is worth noting that the weaker reduction of the measured $J(O^1D)$ compared to the simulated $J(O^1D)$ between 18 and 23 June can also be attributed by a compensation between the optical effect of aerosols, tending to reduce observe $J(O^1D)$, and the thinning ozone column between these two dates (Fig. 2), tending to compensate the effect of dust. This compensation effect between the effects of changes in AOD and in total ozone column on surface UV irradiance, and thus also on $J(O^1D)$, has been discussed by di Sarra et al. (2002), who have shown that during spring and summer at Lampedusa, the synoptic conditions leading to dust transport also induce thinner ozone colums.

Figure 12a confirms that the representation of the diurnal cycle of $J(O^1D)$ at Lampedusa by the Fast-JX module within CHIMERE is very satisfactory. The linear correlation coefficient between the observed and modelled value for the REF simulation is of 0.981, slightly stronger than the value of 0.972 obtained for the NA simulation (Table 3). The high values of these correlation coefficients for both simulations confirm that the general shape of the diurnal cycle of $J(O^1D)$ is captured very well by both simulations, confirming that the dependence of $J(O^1D)$ on the solar zenith angle is represented correctly by the CHIMERE model. The average of the 610 valid data points, representative of average daytime $J(O^1D)$ during the simulation, is lower by 5.8 % when compared to the observations, while the NA simulation has a positive bias of 2.3 %.

3.2.3 Dependence of $J(O^1D)$ and $J(NO_2)$ on the AOD at fixed zenith angle

Finally, in order to evaluate directly the impact of the aerosols on $J(O^1D)$ and $J(NO_2)$, as in Gerasopoulos et al. (2012) and Casasanta et al. (2011), we produced scatter

ACPD
15, 7585–7643, 2015

plots representing the modelled photolysis rates as a function of the modelled AOD at 400 nm for clear sky conditions and for a fixed zenith angle (Fig. 13). These scatter plots have been produced by selecting, for all the model points located at about the same latitude as Lampedusa (35.5 ± 3° N), the times when no clouds are present in the model, and for which the SZA corresponds to the target SZA (30 and 60°) within a tolerance margin of ±1°. As discussed above, the modelled photolysis rates have been muntiplied by $\frac{1}{1+A}$ where A is the albedo, fixed at 0.1 in the model, in order to permit the comparison of the model outputs with measurements that take into account only the downward actinic flux. The size of the dataset for modelled values is very large (12 637 points for panels a and c; 12 916 points for panels b and d) and describe an AOD range from 0 to values that largely exceed unity. The regression lines provided by Gerasopoulos et al. (2012) for $J(NO_2)$ and by Casasanta et al. (2011) have also been superposed to the scatter plots displayed for comparison.

Regarding $J(NO_2)$, Fig. 13b reproduces the linear relationships given in Gerasopoulos et al. (2012) (their Fig. 6) for $J(NO_2)$ vs AOD at 60° zenith angle. The red line concerns the relationship they establish when the AOD is predominantly due to dust, and the blue line for AOD predominantly due to other aerosols. From the location of our modelled points relative to these linear relationships established from measurement data, it can be said that the quasi-linear dependence between $J(NO_2)$ and the AOD for a fixed zenith angle is reproduced very well by the Fast-JX module in CHIMERE. It can also be inferred from this figure that the relationship between $J(NO_2)$ and the AOD proposed by Gerasopoulos et al. (2012) for the cases when dust aerosols predominates seems to be valid much beyond the AOD range observed in their dataset, which only covered AOD values up to 0.65, against 1.9 in Fig. 13b. For a SZA value of 30° (Fig. 13a), the dependence of $J(NO_2)$ on the AOD is also consistent with the results of Gerasopoulos et al. (2012): the Fig. 10 of these authors indicates an effect between 10 and 15 % on $J(NO_2)$ for an AOD value of 0.7, very similar to what we observe on Fig. 13a. At that point, it is worth going back to Table 3. Analysis of the correlation (0.92) and slope (1.13) of the linear regression between observed and simulated daily maxi-

ACPD
15, 7585–7643, 2015

mal values, representative of SZA values ranging between 12 and 13°, shows that, for the very small SZA values corresponding to solar noon conditions at Lampedusa, the effect of the aerosol optical depth on $J(NO_2)$ at very small SZA values is represented realistically as well.

Regarding $J(O^1D)$, panels c and d of Fig. 13 present the scatter plots of $J(O^1D)$ in this study against AOD for cloud-free condition at a SZA of 30 and 60° respectively. The correlation lines provided by Casasanta et al. (2011) (their Table 2) are also reported on these panels, along with the maximal and minimal hypothesis obtained by applying to the slope and intercept values an uncertainty margin of $\pm 2.5\sigma$, where the uncertainty value σ is provided by these authors. We chose to apply the relationships obtained by Casasanta et al. (2011) for a total ozone column of 280–290 DU, which is the closest values to the modelled ozone columns in the present study. At 30°, the simulated relationship between AOD and $J(O^1D)$ in this study is within the uncertainty range of the linear relationships given by Casasanta et al. (2011), with a large spread in modelled data, maybe due to the very different surface temperatures that can be observed across the domain even at a constant latitude. The reduction of $J(O^1D)$ by a unit AOD in the simulated values is of about 25 %, smaller than the value of 38 % that can be obtained from the results of Casasanta et al. (2011) (their Table 2). This seems to indicate that the effect of the AOD on $J(O^1D)$ might be underestimated by the Fast-JX algorithm within the CHIMERE model, which is even more the case for 60° SZA (Fig. 13d), for which the modelled scatter plot is clearly out of the uncertainty range obtained by appling a $\pm 2.5\sigma$ uncertainty margin to the slope given by these authors. Therefore, it seems that the effect of the AOD on $J(O^1D)$ in CHIMERE might be underestimated, particularly for the high SZA values.

3.3 Impact of the aerosols on the concentration of trace gases

Time series of the simulated ozone concentration is shown in Fig. 14a for the Lampedusa station, and compared to measurements. Figure 14a shows that the agreement between model and measurements at Lampedusa for the simulation period is rather

ACPD
15, 7585–7643, 2015

satisfying. the ozone concentrations evolve between 30 and 70 ppb during this period, with a diurnal cycle of about 10 ppb which is captured by the model. The model is also able to capture the low ozone period between 20 June and 5 July, and the higher ozone concentrations before and after that period. Figure 14b shows the net effect of the AOD on ozone concentration at Lampedusa showing that the effect of the AOD on ozone concentration is almost always negative at that location, reaching −2 ppb during the dust outbreak of 20–25 June above Lampedusa, for a simulated AOD about 0.4.

Figure 15 shows the spatial distribution of the aerosol effects on photochemistry averaged over the whole simulated period. The effect of the AOD on both $J(O^1D)$ and $J(NO_2)$ ranges between a few percents for areas in the northern parts of the domain that present a small average AOD, and about 20 % in the areas that are close to the sources of dust in Africa or downwind of them over the tropical Atlantic ocean. Over the whole domain, as could be expected, the average effect of aerosols is to reduce both $J(O^1D)$ and $J(NO_2)$, affecting both rates in a very similar proportion. Regarding the net average effect of the AOD on ozone concentration, the picture is very contrasted (Fig. 15c). Over the Mediterranean Sea, the northeast Atlantic and continental Europe, as well as parts of equatorial Africa, the effect of the reduction in photolytic rates leads to a net average reduction in ozone concentrations, as could be seen for Lampedusa in Fig. 14. This reduction locally reaches 1 ppb over the Mediterranean basin, as well as in areas of equatorial Africa. On the contrary, over the Saharan desert as well as over the tropical Atlantic below the dust plume, ozone concentration seems to be increased by this reduction in the photochemical reaction rates. As discussed in Bian et al. (2003), this change of sign in the effect of AOD on ozone concentrations might be an effect of the competition between reduced ozone formation due to the reduction of $J(NO_2)$, and reduced ozone destruction due to the reduction of $J(O^1D)$, yielding, according to the photochemical regime, to a positive, negative or neutral effect of AOD on ozone concentration. Close to the sources of NO_x in heavily populated and industrialized areas and/or in areas with intense shipping emissions, reduction of $J(NO_2)$ seems to yield a reduction of ozone production, and therefore of ozone concentrations. On the

ACPD
15, 7585–7643, 2015

contrary, in remote areas far away from anthropogenic sources of NO_x, the predominant effect seems to be the reduction of photolytic ozone destruction through $J(O^1D)$, yielding stronger ozone concentrations in the presence of a significant optical depth.

3.4 Sensitivity to a bias in total ozone column

The total ozone column in the model is biased towards low values when compared to observations (Fig. 2). As it is well known that the total ozone column is a critical parameter in simulating accurately the value of $J(O^1D)$ in the troposphere, we performed a sensitivity simulation which identical to the REF simulation except that the calculation of the photolytic rates has been performed after multiplying the ozone concentrations throughout the stratosphere and the troposphere by 1.18, thereby compensating the bias on ozone column visible on Fig. 2. This simulation with enhanced ozone column has been named *O3+*. The effect of this increase of 18 % of the total ozone column is to reduce the modelled $J(O^1D)$ by about 20 % in Lampedusa (Fig. 10) as well as in the rest of the domain (not shown), with a stronger reduction in the northern part of the domain and a weaker reduction in the south. As the bias in $J(O^1D)$ was weak in the REF run (Fig. 10), the $J(O^1D)$ photolytic rates in the *O3+* simulation have a strong negative bias of about 20 % compared to the measured values. The temporal variations of $J(O^1D)$ are not changed very much by this debiasing of ozone column (Fig. 10).

As expected (Fuglestvedt et al., 1994), $J(NO_2)$ values show a very small sensitivity to this debiasing of the ozone column. The increase of 18 % in the model ozone column results in a reduction by about 0.3 % of the average $J(NO_2)$ over the entire domain.

The effect of the modification of the ozone column on ozone concentrations is significant (Fig. 16), with an increase of up to 4 ppb of the ozone concentrations over remote areas such as the Saharan area and the eastern Mediterranean, and a weaker increase of ozone concentrations aver continental Europe. This increase of ozone concentrations can be attributed to the reduction of ozone photolysis due to the increased ozone column and the reduced value of $J(O^1D)$. Interestingly, this reduction of $J(O^1D)$ has the contrary effect over the North Sea, resulting in slightly increased ozone con-

ACPD
15, 7585–7643, 2015

centrations (about 1 ppb). Generally speaking, it is visible in Fig. 16 that in regions having large anthropogenic emissions such as northern Europe, the Po valley and regions with intense shipping in the Mediterranean, Atlantic, North Sea and Baltic Sea, the effect of the reduced $J(O^1D)$ on ozone concentrations is weak, while it is much stronger in areas far away from the main emissions zones.

The fact that taking into account a debiased ozone column creates a negative bias on $J(O^1D)$ suggest that, from a modelling point of view, using Fast-JX version 7.0b as it is provided, even with the fact that the ozone climatology delivered along with the model seems to to be biased, gives better results in terms of photolytic rates than when the total ozone column is debiased. This counterintuitive result indicates that, from a practical point of view, it is better to use Fast-JX 7.0b with the stratospheric ozone column as it is provided, because the $J(O^1D)$ values calculated with a more realistic ozone column are negatively biased. This highlights the conception of Fast-JX as a tool designed to perform fast and accurate calculations of the photolytic rates within a CTM, rather than a tool made to solve exactly every aspect of the radiative transfers in the atmosphere.

4 Conclusions

Two simulations of the atmospheric composition have been performed for the period covering 1 June–15 July 2013, for a large domain including the Mediterranean Sea as well as the surrounding continents and the northeastern part of the Atlantic Ocean. The reference simulation (REF) is the same as described in Menut et al. (2015), while the second simulation is a sensitivity simulation performed without taking into account the optical effect of aerosols on photochemistry (NA simulation). Comparison with MODIS satellite data as well as with AERONET and MFRSR observations shows that the reference simulation reproduces realistic levels of AOD over most of the simulation domain, including the main study area in Lampedusa. Regarding the speciation of the aerosols close to the ground at Lampedusa, these simulations show a good capability to rep-

ACPD
15, 7585–7643, 2015

resent the non-dust PM_{10} concentrations at ground level and their variations, mainly due to sea-salt aerosols. On the contrary, the dust concentrations close to the ground level are too strong in the model compared to the observations, possibly indicating an excess of vertical diffusion and/or sedimentation in the model.

Regarding the photolytic rates, it is shown that both simulations simulate the photolytic rates $J(O^1D)$ and $J(NO_2)$ in a satisfactory way for Lampedusa, when compared to in-situ measurements. The REF simulation is biased by 5.8 % towards an overestimation of the observed $J(O^1D)$ value, and the NA simulation is biased by about 2.3 % towards an overestimation. However, two large uncertainty factors affect the modelled $J(O^1D)$ values: the climatology of stratospheric ozone that has been used for this study did not fit the observed total ozone column, and the temperature in the model was slightly biased as well. Regarding the representation of $J(NO_2)$, the NA simulation exhibits an overestimation of 12.3 % in $J(NO_2)$ compared to observations, which is largely corrected by the inclusion of the aerosols, as reflected by the much smaller bias in the REF simulation (4.8 %). If we turn to the variations of $J(NO_2)$ and $J(O^1D)$ with time, the correlation coefficient between hourly simulated and measured values is excellent for both simulations, always in excess of 0.97, reflecting the fact that the diurnal cycle of $J(O^1D)$ and $J(NO_2)$ is represented very realistically by the Fast-JX module within the CHIMERE model. If we remove the impact of the diurnal cycle by comparing the daily maxima of $J(O^1D)$ and $J(NO_2)$ in both simulations to measurements, it becomes clear that the day-to-day variability of $J(O^1D)$ is represented much better in the REF simulation than in the NA simulation. While the simulation without effect of the aerosols is not able to reproduce any of the observed day-to-day variations in $J(O^1D)$, the daily maxima of $J(O^1D)$ REF simulation are significantly correlated to the observed values. Therefore, despite the strong dependence of $J(O^1D)$ on the total ozone column, it is safe to state that the inclusion of the optical effect of aerosols improves the representation of the evolution of $J(O^1D)$ in the CHIMERE model. Regarding $J(NO_2)$, the added value of including the aerosol effects is more spectacular since $J(NO_2)$ has no strong dependence on the total ozone column (Fuglestvedt et al., 1994). The REF simulations

ACPD
15, 7585–7643, 2015

captures almost exactly the day-to-day variations of $J(NO_2)$ ($R = 0.92$), while the NA simulation does not capture any of these variations, showing that, in the near-absence of clouds, representing correctly the effect of the aerosols is a necessary and sufficient condition to represent the day-to-day variations of $J(NO_2)$.

The relationship between $J(O^1D)$ and the AOD at a constant zenith angle, as well as for $J(NO_2)$ in CHIMERE has been compared to the results of Gerasopoulos et al. (2012) for $J(NO_2)$ and Casasanta et al. (2011) for $J(O^1D)$. This comparison shows that the dependence of $J(NO_2)$ on the AOD as represented by CHIMERE is very similar to the observational results of Gerasopoulos et al. (2012). Our model results indicate a reduction of $J(NO_2)$ by a unit AOD of about 20 % for a SZA value of 30°, and 35 % for a SZA value of 30°. Regarding $J(O^1D)$, comparison of our model results with the in situ measurements of Casasanta et al. (2011) seems to indicate that the effect of the aerosols on $J(O^1D)$ is underestimated in CHIMERE, particularly for high SZA values (30°). However, from a modelling point of view, this caveat is not critical since photochemistry is not very active when the SZA is so high.

Finally, regarding the optical impact of the aerosols on the ozone concentration through the modulation of the photolytic rates, comparison between the REF simulation and the NA simulation shows that, above Lampedusa, the optical effect of the aerosols reduced the ozone concentration by up to 2 ppb during the dust transport episode that occured between 20–25 June above Lampedusa. This result is consistent with the results of Bian et al. (2003), and as these authors we interpret this reduction as an effect of lower photochemical ozone production in Lampedusa and the surrounding marine and continental areas due to reduced photolysis rates. Over other parts of the simulation domain, such as the Saharan desert, the impact of optical screening by mineral dust is, on the contrary, to increase the ozone concentration. This twofold effect of the optical screening of the incoming shortwave radiation by the aerosols might be explained by the balance between the reduction of $J(NO_2)$, which tends to reduce ozone production particularly in zones under anthropogenic influence, and the reduction of $J(O^1D)$, which tends to reduce ozone destruction.

ACPD
15, 7585–7643, 2015

From a modelling point of view, the main conclusion of this study is that including an online representation of the photolysis rates taking into account the real-time simulated aerosol concentrations with a realistic model for radiative transfers such as Fast-JX permits a much better representation of photolytic rates compared to measurements. This is particularly true for $J(NO_2)$: the representation of $J(O^1D)$ is much more complex, particularly due to the effect of the variations in the total ozone column, which are superposed to the variations due to the AOD. The impact on ozone concentrations in the present study is moderate (a few ppb), which might be due to the relatively coarse model resolution. The impact of modulation of photolytic rates by the AOD may very well be more important in urban conditions where important aerosol loads from natural and anthropogenic sources occur at the same time and place as massive emissions of nitrogen oxides.

Acknowledgement. We thank the ChArMEx program (sponsored by CNRS-INSU, ADEME, Météo-France and CEA) as well as the ADRIMED program (sponsored by ANR) for permitting the collection of the relevant field data, the principal investigators of the three AERONET stations that have been used in this study: Daniela Meloni for Lampedusa, Diouri Mohammed and Djamaleddine Chabane for Oujda, Juan Ramon Moreta Gonzalez for Palma de Mallorca. Measurements at Lampedusa during ChArMEx were partly supported by the Italian Ministry for University and Research through the NextData project. The contributions by Lorenzo De Silvestri and Jean-François Doussin are gratefully acknowledged. The authors also wish to thank François Dulac for his careful editorial and scientific review of the initial manuscript.

References

Alfaro, S. C. and Gomes, L.: Modeling mineral aerosol production by wind erosion: emission intensities and aerosol size distributions in source areas, J. Geophys. Res., 106, 18075–18084, doi:10.1029/2000JD900339, 2001. 7592

Bessagnet, B., Hodzic, A., Vautard, R., Beekmann, M., Cheinet, S., Honoré, C., Liousse, C., and Rouil, L.: Aerosol modeling with CHIMERE: preliminary evaluation at the continental scale, Atmos. Environ., 38, 2803–2817, 2004. 7591

ACPD
15, 7585–7643, 2015

Bian, H. and Prather, M.: Fast-J2: accurate simulation of stratospheric photolysis in global chemical models, J. Atmos. Chem., 41, 281–296, 2002. 7589, 7592, 7593

Bian, H. and Zender, C. S.: Mineral dust and global tropospheric chemistry: relative roles of photolysis and heterogeneous uptake, J. Geophys. Res., 108, 4672 doi:10.1029/2002JD003143, 2003. 7589, 7593

Bian, H., Prather, M. J., and Takemura, T.: Tropospheric aerosol impacts on trace gas budgets through photolysis, J. Geophys. Res., 108, 4242, doi:10.1029/2002JD002743, 2003. 7589, 7614, 7618

Bowen, H. J. M.: Environmental Chemistry of the Elements, Academic Press,London, 1979. 7598

Casasanta, G., di Sarra, A., Meloni, D., Monteleone, F., Pace, G., Piacentino, S., and Sferlazzo, D.: Large aerosol effects on ozone photolysis in the Mediterranean, Atmos. Environ., 45, 3937–3943, doi:10.1016/j.atmosenv.2011.04.065 2011. 7588, 7596, 7611, 7612, 7613, 7618, 7640

Davidson, J. A., Cantrell, C. A., Mcdaniel, A. H., Shetter, R. E., Madronich, S., and Calvert, J. G.: Visible-ultraviolet absorption sross sections for NO_2 as a function of temperature, J. Geophys. Res., 93, 7105–7112, 1988. 7596

Di Iorio, T., di Sarra, A., Sferlazzo, D. M., Cacciani, M., Meloni, D., Monteleone, F., Fuà, D., and Fiocco, G.: Seasonal evolution of the tropospheric aerosol vertical profile in the central Mediterranean and role of desert dust, J. Geophys. Res., 114, D02201, doi:10.1029/2008JD010593, 2009. 7597

di Sarra, A., Cacciani, M., Chamard, P., Cornwall, C., DeLuisi, J. J., Di Iorio, T., Disterhoft, P., Fiocco, G., Fuà, D., and Monteleone, F.: Effects of desert dust and ozone on the ultraviolet irradiance at the Mediterranean island of Lampedusa during PAUR II, J. Geophys. Res., 107, PAU 2-1–PAU 2-14, doi:10.1029/2000JD000139, 2002. 7611

di Sarra, A., Sferlazzo, D., Meloni, D., Anello, F., Bommarito, C., Corradini, S., and Di Iorio, T.: Empirical correction of MFRSR aerosol optical depths for the aerosol forward scattering and development of a long-term integrated MFRSR-Cimel dataset at Lampedusa, Appl. Optics, in press, 2015. 7596

Diaz, J., Exposito, F., Torres, C., Herrera, F., Prospero, J., and Romero, M.: Radiative properties of aerosols in Saharan dust outbreaks using ground-based and satellite data: applications to radiative forcing, J. Geophys. Res., 106, 18403–18416, 2001. 7589

ACPD
15, 7585–7643, 2015

Favez, O., Cachier, H., Sciare, J., Alfaro, S. C., El-Araby, T., Harhash, M. A., and Abdelwahab, M. M.: Seasonality of major aerosol species and their transformations in Cairo megacity, Atmos. Environ., 42, 1503–1516, 2008. 7598, 7599

Fuglestvedt, J. S., Jonson, J. E., and Isaksen, I. S. A.: Effects of reductions in stratospheric ozone on tropospheric chemistry through change in photolysis rates, Tellus, 46 B, 172–192, 1994. 7615, 7617

Gardner, E., Sperry, P. D., and Calvert, J. C.: Primary quantum yields of NO_2 photodissociation, J. Geophys. Res., 92, 6642–6652, 1987. 7596

Gerasopoulos, E., Kazadzis, S., Vrekoussis, M., Kouvarakis, G., Liakakou, E., Kouremeti, N., Giannadaki, D., Kanadikou, M., Bohn, B., and Mihalopoulos, N.: Factors affecting O_3 and NO_2 photolysis frequencies measured in the eastern Mediterranean during the five-year period 2002–2006, J. Geophys. Res., 117, D22305, doi:10.1029/2012JD017622, 2012. 7588, 7611, 7612, 7618, 7640

Ginoux, P., Chin, M., Tegen, I., Prospero, J. M., Holben, B., Dubovik, O., and Lin, S. J.: Sources and distributions of dust aerosols simulated with the GOCART model, J. Geophys. Res., 106, 20255–20273, 2001. 7592

Granier, C., Artaxo, P., and Reeves, C. E. (Eds.): Sea-salt aerosol source functions and emissions, in: Emissions of Atmospheric Trace Compounds, Springer Netherlands, 333–359, doi:10.1007/978-1-4020-2167-1_9, 2004. 7606

Guinot, B., Cachier, H., and Oikonomou, K.: Geochemical perspectives from a new aerosol chemical mass closure, Atmos. Chem. Phys., 7, 1657–1670, doi:10.5194/acp-7-1657-2007, 2007. 7598

Hauglustaine, D. A., Hourdin, F., Jourdain, L., Filiberti, M.-A., Walters, S., Lamarque, J.-F., and Holland, E. A.: Interactive chemistry in the Laboratoire de Meteorologie Dynamique general circulation model: description and background tropospheric chemistry evaluation, J. Geophys. Res., 109, D04314, doi:10.1029/2003JD003957, 2004. 7592

Kaufman, Y., Tanré, D., Dubovik, O., Karnieli, A., and Remer, L. A.: Absorption of sunlight by dust as inferred from satellite and ground-based remote sensing, Geophys. Res. Lett., 28, 1479–1482, 2001. 7589

Keene, W. C., Sander, R., Pszenny, A. A. P., Vogt, R., Crutzen, P. J., and Galloway, J. N.: Aerosol pH in the marine boundary layer: a review and model evaluation, J. Aerosol Sci., 29, 339–356, 1998. 7598

ACPD
15, 7585–7643, 2015

Kinne, S., Lohmann, U., Feichter, J., Schulz, M., Timmreck, C., Ghan, S., Easter, R., Chin, M., Ginoux, P., Takemura, T., Tegen, I., Koch, D., Herzog, M., Penner, J., Pitari, G., Holben, B., Eck, T., Smirnov, A., Dubovik, O., Slutsker, I., Tanre, D., Torres, O., Mishchenko, M., Geogdzhayev, I., Chu, D. A., and Kaufman, Y.: Monthly averages of aerosol properties: a global comparison among models, satellite data, and AERONET ground data, J. Geophys. Res., 108, AAC 3-1 – AAC 3-42, doi:10.1029/2001JD001253, 2003. 7593

Kishcha, P., Nickovic, S., Starobinets, B., di Sarra, A., Udisti, R., Becagli, S., Sferlazzo, D., Bommarito, C., and Alpert, P.: Sea-salt aerosol forecasts compared with daily measurements at the island of Lampedusa (Central Mediterranean), Atmos. Res., 100, 28–35, 2011. 7598

Mailler, S., Khvorostyanov, D., and Menut, L.: Impact of the vertical emission profiles on background gas-phase pollution simulated from the EMEP emissions over Europe, Atmos. Chem. Phys., 13, 5987–5998, doi:10.5194/acp-13-5987-2013, 2013. 7589

Marconi, M., Sferlazzo, D. M., Becagli, S., Bommarito, C., Calzolai, G., Chiari, M., di Sarra, A., Ghedini, C., Gómez-Amo, J. L., Lucarelli, F., Meloni, D., Monteleone, F., Nava, S., Pace, G., Piacentino, S., Rugi, F., Severi, M., Traversi, R., and Udisti, R.: Saharan dust aerosol over the central Mediterranean Sea: PM_{10} chemical composition and concentration versus optical columnar measurements, Atmos. Chem. Phys., 14, 2039–2054, doi:10.5194/acp-14-2039-2014, 2014. 7598

Marticorena, B. and Bergametti, G.: Modelling the atmospheric dust cycle: 1-design a soil-derived dust emissions scheme, J. Geophys. Res., 100, 16415–16430, 1995. 7592

McPeters, R., Labow, G., and Johnson, B. J.: A satellite-derived ozone climatology for balloonsonde estimation of total column ozone, J. Geophys. Res., 102, 8875–8885, 1997. 7589, 7594

Meloni, D., di Sarra, A., Herman, J. R., Monteleone, F., and Piacentino, S.: Comparison of ground-based and TOMS erythemal UV doses at the island of Lampedusa in the period 1998–2003, J. Geophys. Res., 110, D01202, doi:10.1029/2004JD005283, 2005. 7594

Menut, L., Bessagnet, B., Khvorostyanov, D., Beekmann, M., Blond, N., Colette, A., Coll, I., Curci, G., Foret, G., Hodzic, A., Mailler, S., Meleux, F., Monge, J.-L., Pison, I., Siour, G., Turquety, S., Valari, M., Vautard, R., and Vivanco, M. G.: CHIMERE 2013: a model for regional atmospheric composition modelling, Geosci. Model Dev., 6, 981–1028, doi:10.5194/gmd-6-981-2013, 2013. 7589, 7591

Menut, L., Mailler, S., Siour, G., Bessagnet, B., Turquety, S., Rea, G., Briant, R., Mallet, M., Sciare, J., and Formenti, P.: Analysis of the atmospheric composition during the summer

ACPD
15, 7585–7643, 2015

2013 over the Mediterranean area using the CHARMEX measurements and the CHIMERE model, Atmos. Chem. Phys. Discuss., 14, 23075–23123, doi:10.5194/acpd-14-23075-2014, 2014. 7589, 7590, 7591, 7592, 7601, 7616

Michalakes, J., Dudhia, J., Gill, D., Henderson, T., Klemp, J., Skamarock, W., and Wang, W.: The weather research and forecast model: software architecture and performance, in: Proceedings of the Eleventh ECMWF Workshop on the Use of High Performance Computing in Meteorology, edited by: Zwieflhofer, W. and Mozdzynski, G., World Scientific, Singapore, 269–276, 2005. 7591

Michel Flores, J., Bar-Or, R. Z., Bluvshtein, N., Abo-Riziq, A., Kostinski, A., Borrmann, S., Koren, I., Koren, I., and Rudich, Y.: Absorbing aerosols at high relative humidity: linking hygroscopic growth to optical properties, Atmos. Chem. Phys., 12, 5511–5521, doi:10.5194/acp-12-5511-2012, 2012. 7593

Mischenko, M., Travis, L. D., and Lacis, A. A.: Scattering, Absorption and Emission of Light by Small Particles, Cambridge University Press, Cambridge, 2002. 7593

Pace, G., di Sarra, A., Meloni, D., Piacentino, S., and Chamard, P.: Aerosol optical properties at Lampedusa (Central Mediterranean). 1. Influence of transport and identification of different aerosol types, Atmos. Chem. Phys., 6, 697–713, doi:10.5194/acp-6-697-2006, 2006. 7588, 7595, 7596, 7606

Putaud, J.-P., Van Dingenen, R., Dell'Acqua, A., Raes, F., Matta, E., Decesari, S., Facchini, M. C., and Fuzzi, S.: Size-segregated aerosol mass closure and chemical composition in Monte Cimone (I) during MINATROC, Atmos. Chem. Phys., 4, 889–902, doi:10.5194/acp-4-889-2004, 2004. 7598

Real, E. and Sartelet, K.: Modeling of photolysis rates over Europe: impact on chemical gaseous species and aerosols, Atmos. Chem. Phys., 11, 1711–1727, doi:10.5194/acp-11-1711-2011, 2011. 7589

Remer, L. A., Kleidman, R. G., Levy, R. C., Kaufman, Y. J., Tanré, D., Mattoo, S., Vanderleimartins, J., Ichoku, C., Koren, I., Yu, H., and Holben, B. N.: Global aerosol climatology from the MODIS satellite sensors, J. Geophys. Res., 113, D14S07,doi:10.1029/2007JD009661, 2008. 7597

Savoie, D. L., Maring, H. B., Izaguirre, M. A., Snowdon, T., and Custals, L.: Ground-based measurements of aerosol chemical, physical and optical properties during the Puerto Rico Dust Experiment (PRIDE), EOS T. Am. Geophys. Un., 81(48), Fall Meet. Suppl., F44, 2000. 7589

ACPD
15, 7585–7643, 2015

Sayer, A. M., Hsu, N. C., Bettenhausen, C., and Jeong, M.-J.: Validation and uncertainty estimates for MODIS collection 6 “Deep Blue” aerosol data, J. Geophys. Res., 118, 7864–7872, 2013. 7597

Scheuvens, D., Schütz, L., Kandler, K., Ebert, M., and Weinbruch, S.: Bulk composition of northern African dust and its source sediments – a compilation, Earth-Sci. Rev., 116, 170–194, 2013. 7598

Sciare, J., Oikonomou, K., Cachier, H., Mihalopoulos, N., Andreae, M. O., Maenhaut, W., and Sarda-Estève, R.: Aerosol mass closure and reconstruction of the light scattering coefficient over the Eastern Mediterranean Sea during the MINOS campaign, Atmos. Chem. Phys., 5, 2253–2265, doi:10.5194/acp-5-2253-2005, 2005. 7598, 7599

Telford, P. J., Abraham, N. L., Archibald, A. T., Braesicke, P., Dalvi, M., Morgenstern, O., O’Connor, F. M., Richards, N. A. D., and Pyle, J. A.: Implementation of the Fast-JX Photolysis scheme (v6.4) into the UKCA component of the MetUM chemistry-climate model (v7.3), Geosci. Model Dev., 6, 161–177, doi:10.5194/gmd-6-161-2013, 2013. 7589

Turquety, S., Menut, L., Bessagnet, B., Anav, A., Viovy, N., Maignan, F., and Wooster, M.: APIFLAME v1.0: high-resolution fire emission model and application to the Euro-Mediterranean region, Geosci. Model Dev., 7, 587–612, doi:10.5194/gmd-7-587-2014, 2014. 7592

Vuolo, M. R., Menut, L., and Chepfer, H.: Impact of transport schemes on modeled dust concentrations, J. Atmos. Ocean. Tech., 26, 1135–1143, 2009. 7607

Wild, O., Zhu, X., and Prather, J.: Fast-J: accurate simulation of the in- and below-cloud photolysis in tropospheric chemical models, J. Atmos. Chem., 37, 245–282, 2000. 7589, 7592, 7593

ACPD
15, 7585–7643, 2015

Table 1. Dectional bins for aerosols.

bin number	Diameter range (µm)
1	0.039–0.078
2	0.078–0.15
3	0.15–0.31
4	0.31–0.625
5	0.62–1.25
6	1.25–2.50
7	2.50–5.00
8	5.00–10.00
9	10.00–20.00
10	20.00–40.00

ACPD
15, 7585–7643, 2015

Table 2. Refractive indices used for mineral dust.

λ (nm)	Refractive index
200	$1.53 + 5.5 \times 10^{-3} i$
300	$1.53 + 5.5 \times 10^{-3} i$
400	$1.53 + 2.4 \times 10^{-3} i$
600	$1.53 + 8.9 \times 10^{-4} i$
1000	$1.53 + 7.4 \times 10^{-4} i$

ACPD
15, 7585–7643, 2015

Table 3. Statistical scores for the regression of hourly modelled $J(O^1D)$ and $J(NO_2)$ values against measurements, for hourly values and daily maxima.

	$J(O^1D)$				$J(NO_2)$			
	Hourly values		Daily maxima		Hourly values		Daily maxima	
	REF	NA	REF	NA	REF	NA	REF	NA
N	610	610	26	26	698	698	26	26
slope	0.98	1.02	0.31	0.05	1.09	1.07	1.13	−0.005
R	0.981	0.972	0.46	0.09	0.993	0.987	0.92	−0.05
p	$< 10^{-10}$	$< 10^{-10}$	0.02	0.65	$< 10^{-10}$	$< 10^{-10}$	$< 10^{-10}$	0.81
Bias (%)	−5.8	+2.3	−1.8	+5.3	+4.8	+12.9	+8.2	+12.3

ACPD
15, 7585–7643, 2015

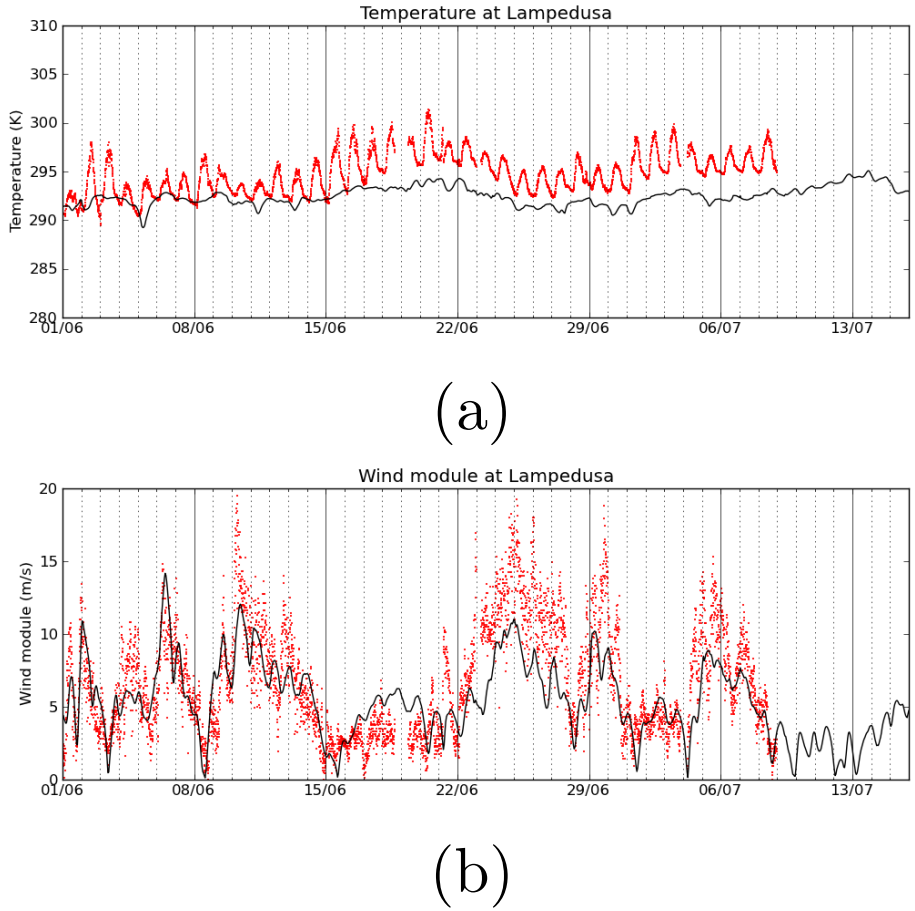

Figure 1. (a) Modelled temperature at Lampedusa (K, black line), and measured temperature (red points); and **(b)**, same as **(a)** for the module of the wind at Lampedusa ($m\,s^{-1}$).

ACPD
15, 7585–7643, 2015

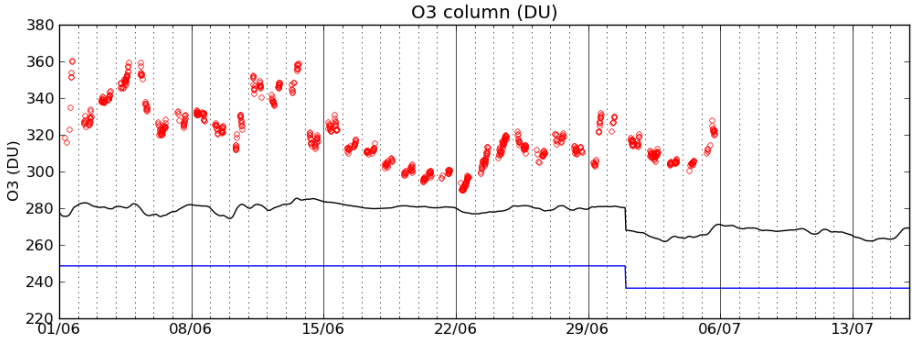

Figure 2. Modelled total (black line) and stratospheric (blue line) ozone column above Lampedusa, expressed in Dobson Units (DU), compared to the measured values (red circles).

ACPD
15, 7585–7643, 2015

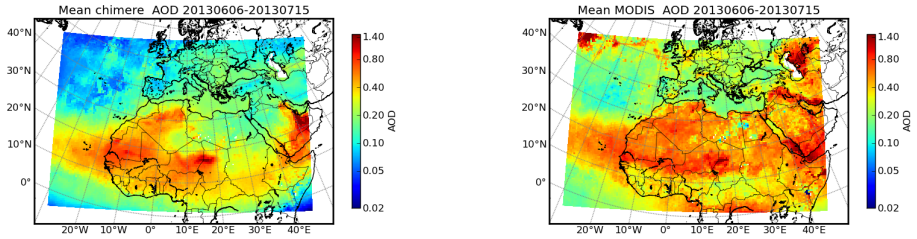

Figure 3. Aerosol optical depth at 600 nm in the CHIMERE model (left column) and at 550 nm as observed by MODIS AQUA and TERRA, averaged from 1 June 2013 to 15 July 2013. Only the points where MODIS data are available are taken into account in the averaging procedure for the CHIMERE data.

ACPD
15, 7585–7643, 2015

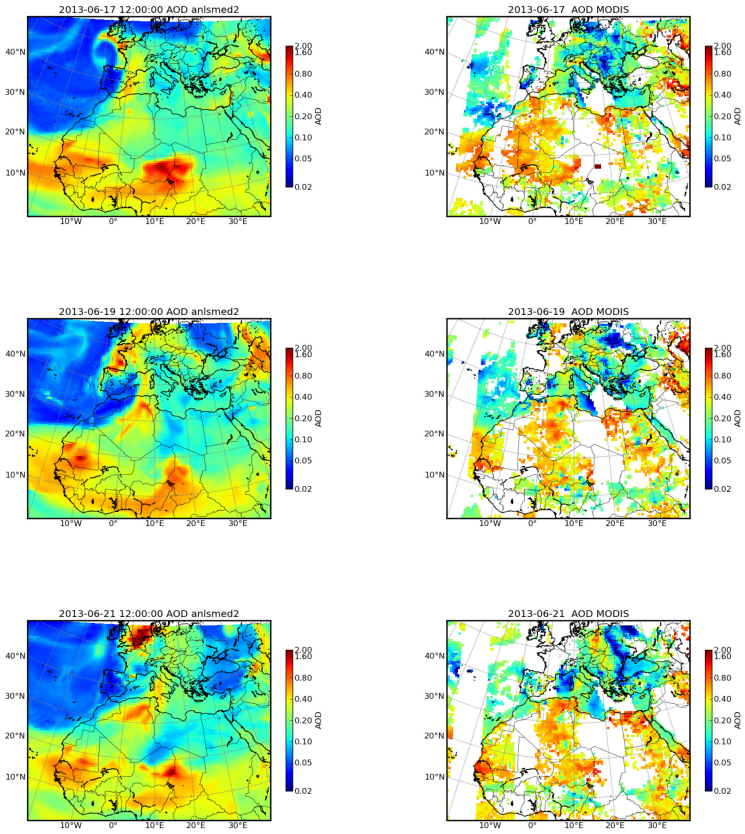

Figure 4. Aerosol optical depth at 600 nm in the CHIMERE model (left column) and at 550 nm as observed by MODIS AQUA and TERRA, for 17 June, 19 and 21, 2013.

ACPD
15, 7585–7643, 2015

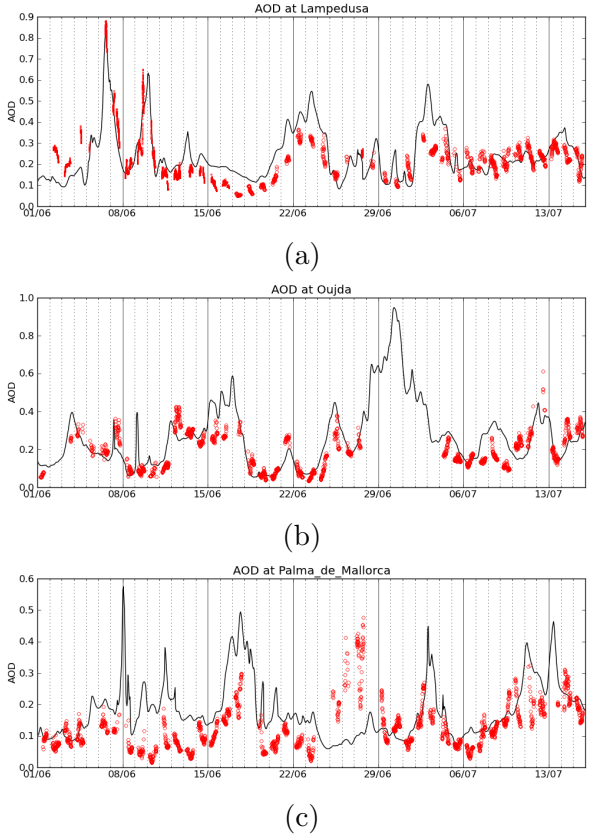

Figure 5. Evolution of AOD (black lines) at 400 nm above Lampedusa, Oujda and Palma de Mallorca, compared to the AERONET AOD interpolated at 400 nm (red circles). For Lampedusa, AERONET data is completed with MFRSR data (red dots) when the AERONET data was not available.

ACPD
15, 7585–7643, 2015

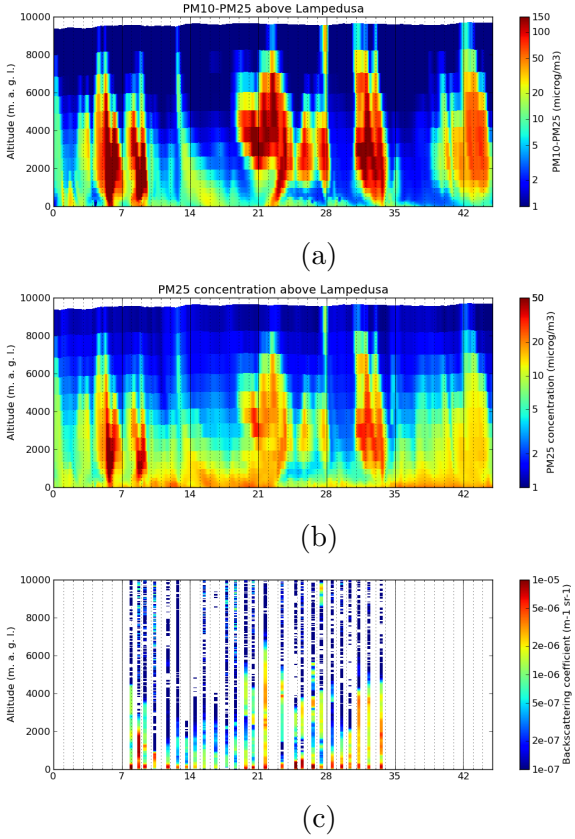

Figure 6. (a) Evolution of modelled $PM_{2.5}$ concentrations above Lampedusa. Horizontal axis: days since 1 June 2013; **(b)** same as **(a)** but for PM_{10}–$PM_{2.5}$; and **(c)**: Lidar backscatter coefficient above Lampedusa. Each selected LIDAR profile is represented by a column of fixed width centered on the instant of the measurement, representing the backscatter coefficient (color levels).

ACPD
15, 7585–7643, 2015

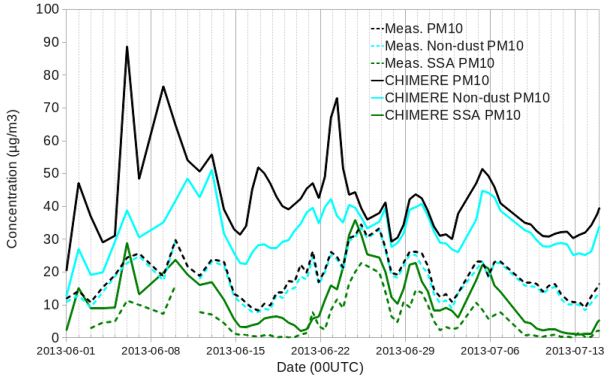

Figure 7. Modelled speciation of PM_{10} aerosols in the first model layer compared to measurements for total PM_{10} (black lines), non-dust PM_{10} (blue lines) and sea-salt aerosols (green lines).

ACPD
15, 7585–7643, 2015

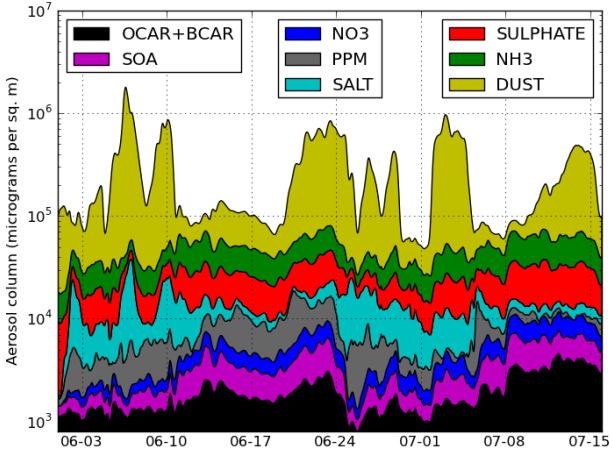

Figure 8. Cumulative plot of the total aerosol mass load ($\mu g\,m^{-2}$) for the following groups of species: organic and black carbon (OCAR+BCAR), secondary organic aerosols (SOA), nitrates (NO_3), primary anthropogenic particulate matter (PPM), sea-salt (SALT), sulphate, ammonium (NH_3) and mineral dust (DUST).

ACPD
15, 7585–7643, 2015

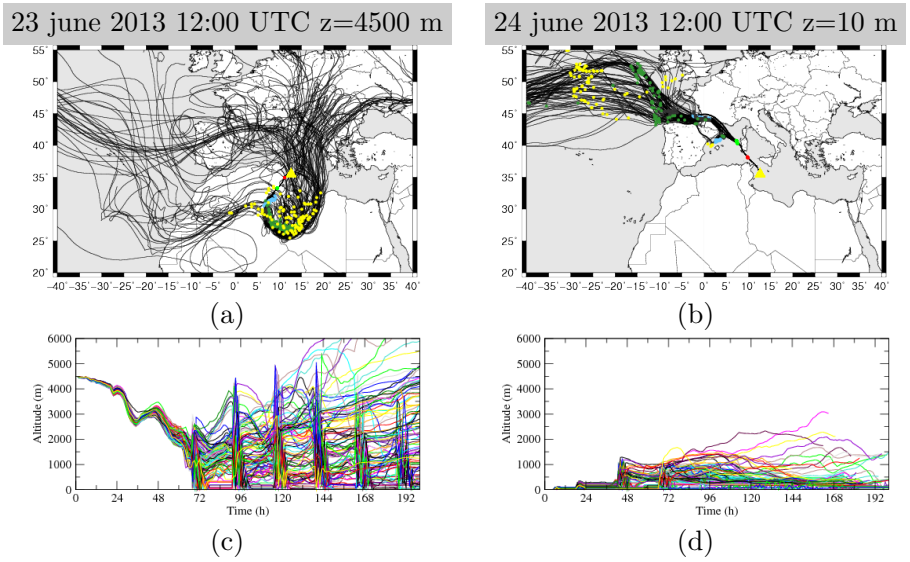

Figure 9. (a) Backplume starting above Lampedusa for 23 June, 12:00 UTC at 4500 m altitude. The yellow triangle represents Lampedusa, the starting location of the backplume. The colored dots correspond to the number of hours before the starting time: red = 12, green = 24, blue = 48, dark green = 72, yellow = 96 **(b)** same as **(a)** but for 24 June, 12:00 UTC at 10 m altitude. **(c)** Altitude of the backplume starting above Lampedusa for 23 June, 12:00 UTC at 4500 m altitude, and **(d)**, altitude of the backplume starting above Lampedusa for 24 June, 12:00 UTC at 10 m altitude.

ACPD
15, 7585–7643, 2015

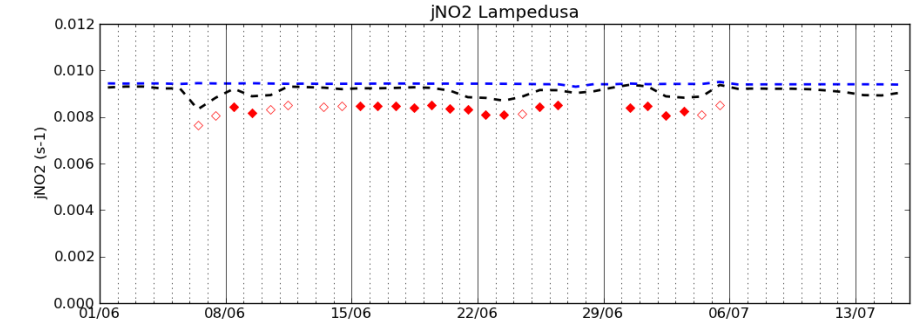

(a)

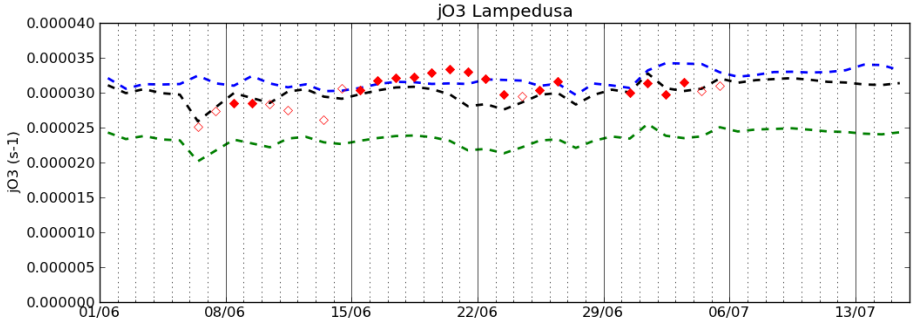

(b)

Figure 10. (a) Daily maximal values of modelled $J(NO_2)$ in s^{-1} for the REF simulation (black dashed line) and the NA simulation (blue dashed line), and measured values of the daily maxima (red diamonds). The days when significant effect of clouds was visible on the spectrometer measurements are signalled on the plot by an empty red diamond. **(b)** same as **(a)** for $J(O^1D)$. The green dashed line represents the $J(O^1D)$ values in the *O3+* simulation.

ACPD
15, 7585–7643, 2015

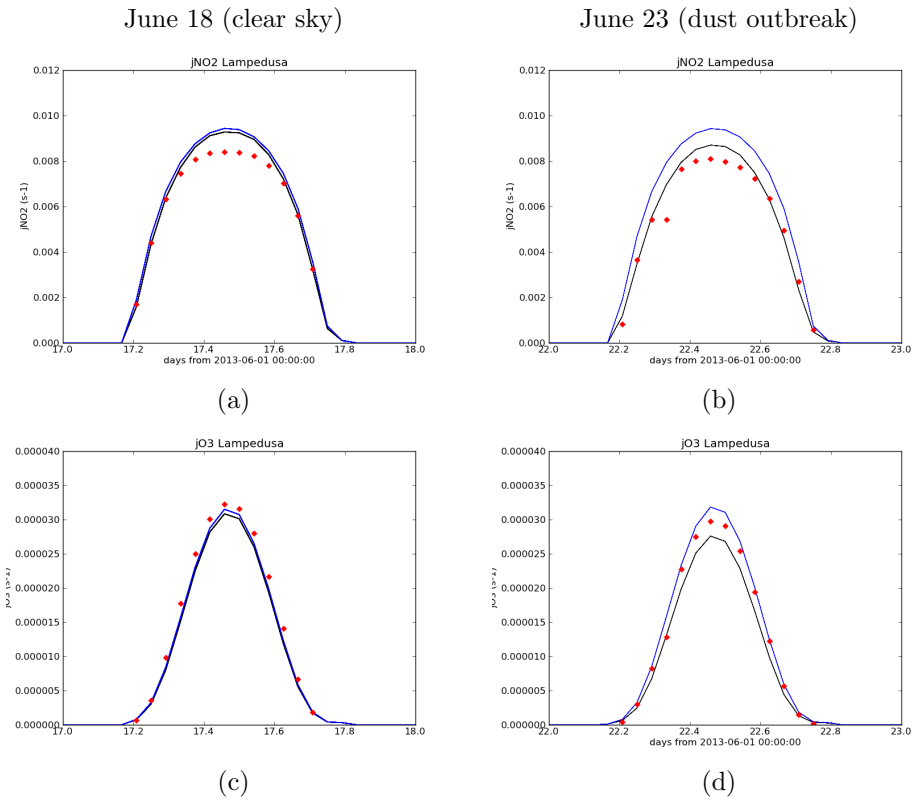

Figure 11. (a) Hourly modelled values of $J(NO_2)$ in the REF simulation (black line) and in the NA simulation (blue line), and hourly measured values of $J(NO_2)$ (red diamonds), for 18 June 2013. **(b)** same as **(a)** but for 23 June; **(c)**: hourly modelled values of $J(O^1D)$ in the REF simulation (black line) and in the NA simulation (blue line), and hourly measured values of $J(O^1D)$ (red diamonds), for 18 June 2013; and **(d)**: same as **(c)** but for 23 June.

ACPD
15, 7585–7643, 2015

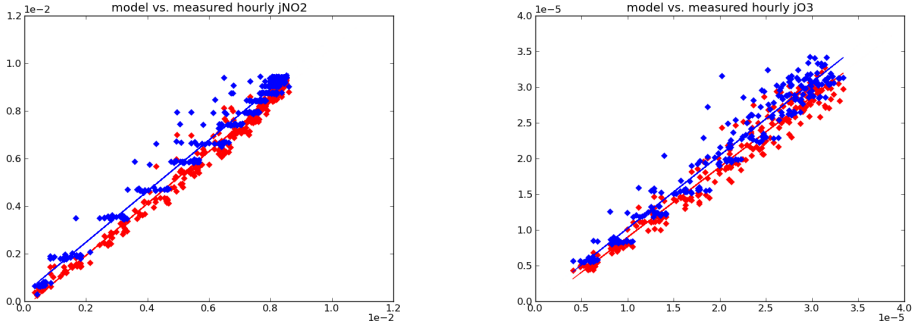

(a) (b)

Figure 12. (a) Scatter plot of hourly modelled $J(NO_2)$ vs. measured $J(NO_2)$ at Lampedusa for 698 points with valid daytime measurements of $J(NO_2)$. Red diamonds represent the $J(NO_2)$ values in the REF simulation, blue diamonds the $J(NO_2)$ values in the NA simulation, with the respective regression lines; **(b)** same as **(a)** for $J(O^1D)$, with 610 valid data points.

ACPD
15, 7585–7643, 2015

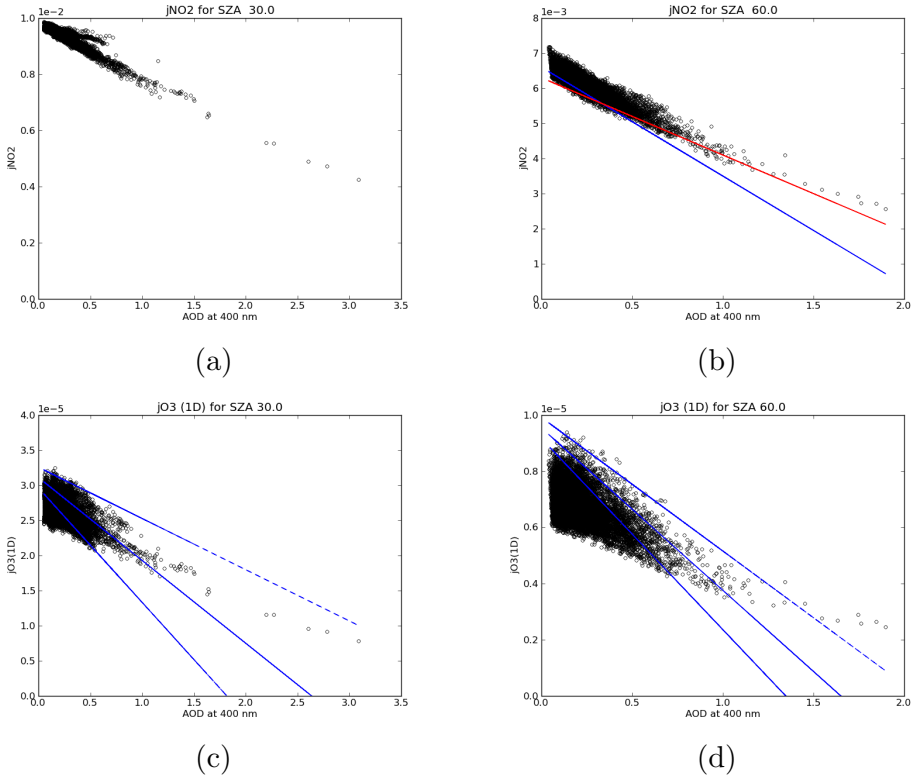

Figure 13. Scatter plots of $J(NO_2)$ **(a, b)** and jO3(1 d) **(c, d)** at the lowest model level vs. the AOD, for clear-sky conditions ant latitudes comprised between 32.5 and 38.5° N. For the purpose of comparison, on panel **(b)**, the regression relationships found by Gerasopoulos et al. (2012) with field data are reported in blue (non-dust aerosols) and red (dust aerosols). On panels **(c, d)** the regression lines by Casasanta et al. (2011) are indicated along with their uncertainty margin.

ACPD
15, 7585–7643, 2015

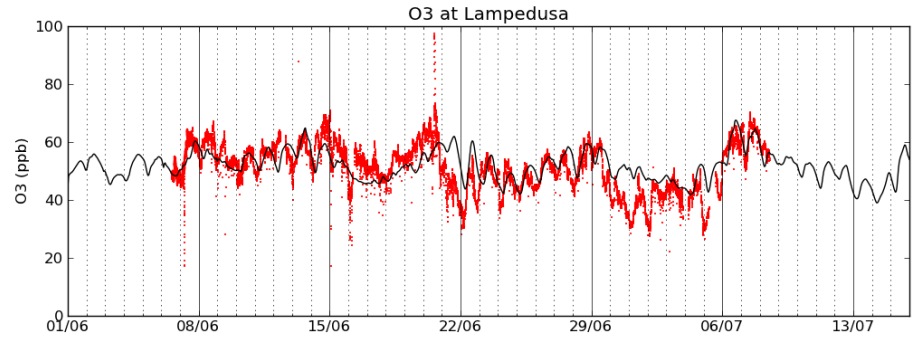

(a)

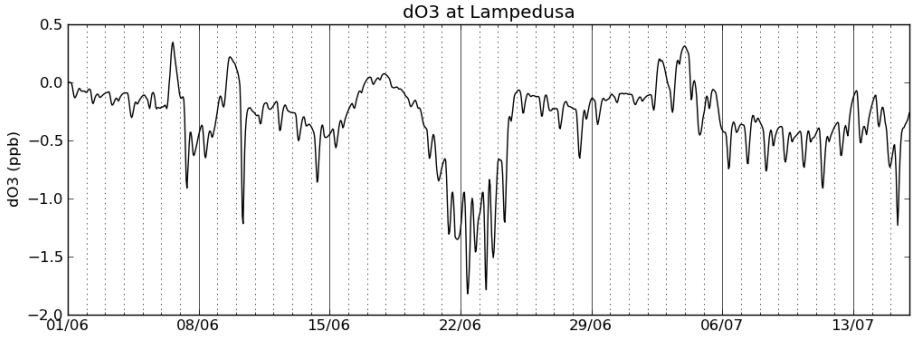

(b)

Figure 14. (a) Time series for ozone concentration (ppb) in the reference simulation in Lampedusa (black line) along with measured values (red dots); and **(b)**, effect of the optical screening by the aerosols on the ozone concentration, computed as $dO_3 = [O_3]_{ref} - [O_3]_{NA}$.

ACPD
15, 7585–7643, 2015

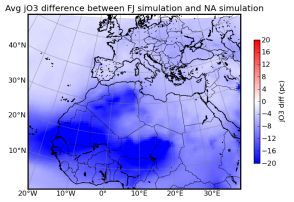

(a)

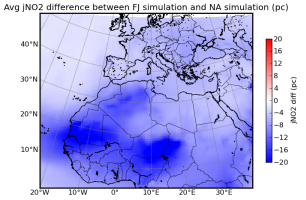

(b)

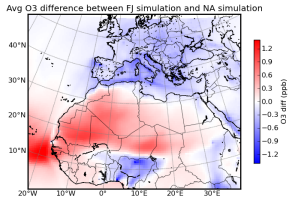

(c)

Figure 15. (a) Average difference of $J(O^1D)$ between REF and NA (%) for all the simulation period (1 June–15 July); **(b)** average difference of $J(NO_2)$ between REF and NA (%) for all the simulation period; and **(c)** average difference of ozone concentration between REF and NA for all the simulation period (ppb).

ACPD
15, 7585–7643, 2015

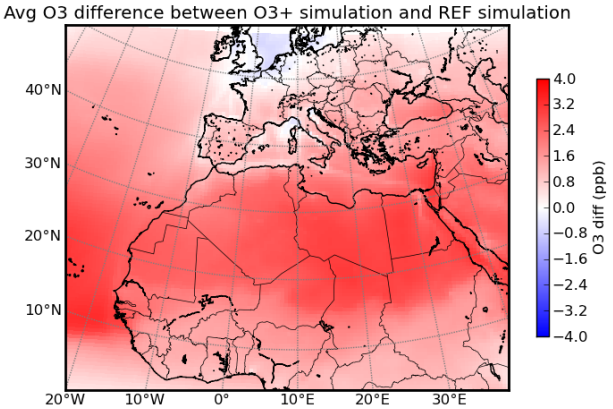

Figure 16. Difference (ppb) in the concentration of ozone in the lowest model layer between the *O3+* simulation and the REF simulation.

ACPD
15, 7585–7643, 2015